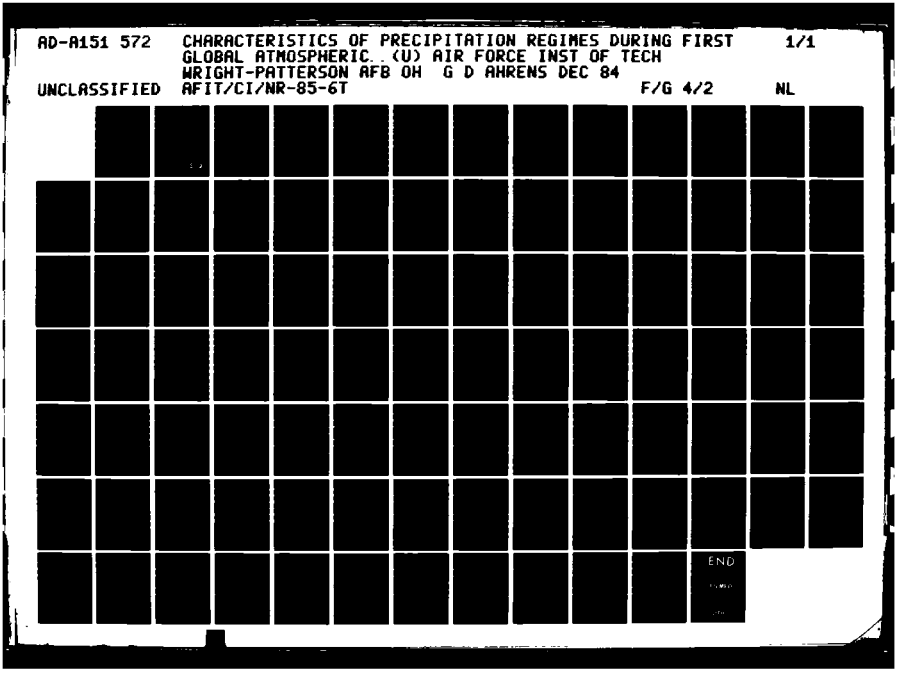
AD-A151 572 CHARACTERISTICS OF PRECIPITATION REGIMES DURING FIRST 1/1
GLOBAL ATMOSPHERIC.. (U) AIR FORCE INST OF TECH
WRIGHT-PATTERSON AFB OH G D AHRENS DEC 84
UNCLASSIFIED AFIT/CI/NR-85-6T F/G 4/2 NL
END

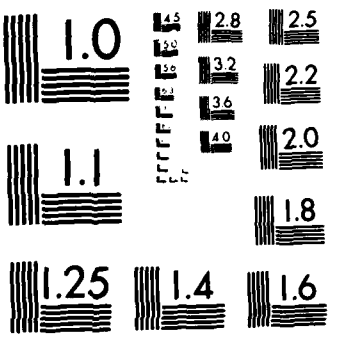

MICROCOPY RESOLUTION TEST CHART
NATIONAL BUREAU OF STANDARDS 1963 A

UNCLASS

SECURITY CLASSIFICATION OF THIS PAGE (When Data Entered)

REPORT DOCUMENTATION PAGE	READ INSTRUCTIONS BEFORE COMPLETING FORM
1. REPORT NUMBER: AFIT/CI/NR 85-6T	3. RECIPIENT'S CATALOG NUMBER
4. TITLE (and Subtitle): Characteristics Of Precipitation Regimes During First Global Atmospheric Research Project Global Experiments	5. TYPE OF REPORT & PERIOD COVERED: THESIS/DISSERTATION
	6. PERFORMING ORG. REPORT NUMBER
7. AUTHOR(s): Glenn David Ahrens	8. CONTRACT OR GRANT NUMBER(s)
9. PERFORMING ORGANIZATION NAME AND ADDRESS: AFIT STUDENT AT: The University of Utah	10. PROGRAM ELEMENT, PROJECT, TASK AREA & WORK UNIT NUMBERS
11. CONTROLLING OFFICE NAME AND ADDRESS: AFIT/NR WPAFB OH 45433	12. REPORT DATE: 1984
	13. NUMBER OF PAGES: 73
14. MONITORING AGENCY NAME & ADDRESS (if different from Controlling Office)	15. SECURITY CLASS. (of this report): UNCLASS
	15a. DECLASSIFICATION/DOWNGRADING SCHEDULE

16. DISTRIBUTION STATEMENT (of this Report)

APPROVED FOR PUBLIC RELEASE; DISTRIBUTION UNLIMITED

17. DISTRIBUTION STATEMENT (of the abstract entered in Block 20, if different from Report)

18. SUPPLEMENTARY NOTES

APPROVED FOR PUBLIC RELEASE: IAW AFR 190-1

LYNN E. WOLAVER 27 Feb 85
Dean for Research and
Professional Development
AFIT, Wright-Patterson AFB OH

19. KEY WORDS (Continue on reverse side if necessary and identify by block number)

20. ABSTRACT (Continue on reverse side if necessary and identify by block number)

ATTACHED

DTIC ELECTE S MAR 25 1985 D

DD FORM 1473 EDITION OF 1 NOV 65 IS OBSOLETE

SECURITY CLASSIFICATION OF THIS PAGE (When Data Entered)

85 03 11 069

AD-A151 572

DTIC FILE COPY

DISCLAIMER NOTICE

THIS DOCUMENT IS BEST QUALITY PRACTICABLE. THE COPY FURNISHED TO DTIC CONTAINED A SIGNIFICANT NUMBER OF PAGES WHICH DO NOT REPRODUCE LEGIBLY.

ABSTRACT

Precipitation data are obtained from the GWE (Global Weather Experiment) FGGE (First GARP (Global Atmospheric Research Project) Global Experiment) data sets observed from December 1978 through November 1979. The FGGE precipitation data are compared to climatological data and other fields compiled or calculated from the FGGE data. These other fields are the U and V wind components, heating fields, velocity potentials, and stream functions. The precipitation data are edited and put into a useful global format. The 1979 data are compared to climatology. The precipitation fields generally agree with more extensive climatologies, though some important regional differences are noted. Large scale overturning circulations are colocated with extensive areas of precipitation in the tropics.

The analysis of rainfall is adversely affected by the sparse data density over the oceans and in remote areas. In the future, the precipitation data should be combined with and scrutinized against satellite data, especially over the oceans.

AFIT RESEARCH ASSESSMENT

The purpose of this questionnaire is to ascertain the value and/or contribution of research accomplished by students or faculty of the Air Force Institute of Technology (AU). It would be greatly appreciated if you would complete the following questionnaire and return it to:

AFIT/NR
Wright-Patterson AFB OH 45433

RESEARCH TITLE: Characteristics Of Precipitation Regimes During First Global Atmospheric Research Project Global Experiments

AUTHOR: Glenn David Ahrens

RESEARCH ASSESSMENT QUESTIONS:

1. Did this research contribute to a current Air Force project?

( ) a. YES ( ) b. NO

2. Do you believe this research topic is significant enough that it would have been researched (or contracted) by your organization or another agency if AFIT had not?

( ) a. YES ( ) b. NO

3. The benefits of AFIT research can often be expressed by the equivalent value that your agency achieved/received by virtue of AFIT performing the research. Can you estimate what this research would have cost if it had been accomplished under contract or if it had been done in-house in terms of manpower and/or dollars?

( ) a. MAN-YEARS _____ ( ) b. $_____

4. Often it is not possible to attach equivalent dollar values to research, although the results of the research may, in fact, be important. Whether or not you were able to establish an equivalent value for this research (3. above), what is your estimate of its significance?

( ) a. HIGHLY SIGNIFICANT ( ) b. SIGNIFICANT ( ) c. SLIGHTLY SIGNIFICANT ( ) d. OF NO SIGNIFICANCE

5. AFIT welcomes any further comments you may have on the above questions, or any additional details concerning the current application, future potential, or other value of this research. Please use the bottom part of this questionnaire for your statement(s).

NAME GRADE POSITION

ORGANIZATION LOCATION

STATEMENT(s):

CHARACTERISTICS OF PRECIPITATION REGIMES DURING FIRST GLOBAL ATMOSPHERIC RESEARCH PROJECT GLOBAL EXPERIMENTS

by

Glenn David Ahrens
Captain, Air Force, 1984, 73 pages

Master of Science

The University of Utah

CHARACTERISTICS OF PRECIPITATION REGIMES DURING FIRST GLOBAL ATMOSPHERIC RESEARCH PROJECT GLOBAL EXPERIMENTS

by

Glenn David Ahrens
Captain, Air Force, 1984, 73 pages

Master of Science

The University of Utah

ABSTRACT

Precipitation data are obtained from the GWE (Global Weather Experiment) FGGE (First GARP (Global Atmospheric Research Project) Global Experiment) data sets observed from December 1978 through November 1979. The FGGE precipitation data are compared to climatological data and other fields compiled or calculated from the FGGE data. These other fields are the U and V wind components, heating fields, velocity potentials, and stream functions. The precipitation data are edited and put into a useful global format. The 1979 data are compared to climatology. The precipitation fields generally agree with more extensive climatologies, though some important regional differences are noted. Large scale overturning circulations are colocated with extensive areas of precipitation in the tropics.

The analysis of rainfall is adversely affected by the sparse data density over the oceans and in remote areas. In the future, the precipitation data should be combined with and scrutinized against satellite data, especially over the oceans.

CHARACTERISTICS OF PRECIPITATION REGIMES DURING FIRST GLOBAL ATMOSPHERIC RESEARCH PROJECT GLOBAL EXPERIMENTS

by

Glenn David Ahrens

A thesis submitted to the faculty of
The University of Utah
in partial fulfillment of the requirements for the degree of

Master of Science

Department of Meteorology

The University of Utah

December 1984

THE UNIVERSITY OF UTAH GRADUATE SCHOOL

FINAL READING APPROVAL

To the Graduate Council of The University of Utah.

I have read the dissertation of Glenn D. Ahrens in its final form and have found that (1) its format, citations, and bibliographic style are consistent and acceptable; (2) its illustrative materials including figures, tables, and charts are in place; and (3) the final manuscript is satisfactory to the Supervisory Committee and is ready for submission to the Graduate School.

9/25/84
Date

Julia N. Paegle
Member, Supervisory Committee

Approved for the Major Department

J.E. Geisler
Chairman/Dean

Approved for the Graduate Council

James L. Clayton
Dean of The Graduate School

THE UNIVERSITY OF UTAH GRADUATE SCHOOL

SUPERVISORY COMMITTEE APPROVAL

of a thesis submitted by

Glenn D. Ahrens

This thesis has been read by each member of the following supervisory committee and by majority vote has been found to be satisfactory

9/14/84 — Chairman: Julia N. Paegle

9/14/84 — K.N. Liou

9/14/84 — Jan Paegle

ABSTRACT

Precipitation data are obtained from the GWE (Global Weather Experiment) FGGE (First GARP (Global Atmospheric Research Project) Global Experiment) data sets observed from December 1978 through November 1979. The FGGE precipitation data are compared to climatological data and other fields compiled or calculated from the FGGE data. These other fields are the U and V wind components, heating fields, velocity potentials, and stream functions. The precipitation data are edited and put into a useful global format. The 1979 data are compared to climatology. The precipitation fields generally agree with more extensive climatologies, though some important regional differences are noted. Large scale overturning circulations are colocated with extensive areas of precipitation in the tropics.

The analysis of rainfall is adversely affected by the sparse data density over the oceans and in remote areas. In the future, the precipitation data should be combined with and scrutinized against satellite data, especially over the oceans.

My thesis is dedicated to my wife and family for the long hours, support, and assistance during the writing of this thesis.

TABLE OF CONTENTS

ACKNOWLEDGEMENTS

I would like to express my appreciation to my committee members: Professors Julia N. Paegle, Jan Paegle, and Kuo-Nan Liou, for their support and guidance during the preparation of this thesis. I would especially like to thank Julia N. Paegle for the many hours of assistance she has given throughout my research.

I would also like to thank Greg Dodd, Jeff Koenig, Michael Griffen, Tyree Wilde, and Richard Petrilla for all the extra help given towards the writing of this thesis.

Thanks should also go out to the rest of my fellow students who encouraged me throughout my studies.

Research reported in this thesis has been supported jointly by the National Science Foundation, the National Oceanic and Atmospheric Administration, and the National Aeronautics and Space Administration under Grant Numbers ATM 8219198 and NAG 5-127.

CHAPTER 1

INTRODUCTION

1.1 Motivation

Interest in the global aspects of tropical meteorology has expanded markedly in the last decade. The expansion from hemispheric to global domains of integration of numerical models in operational meteorological centers gave incentive to studies aimed to improve our understanding of large scale tropical circulations. The effect of tropical motions in extratropical flows became apparent as these centers extended their forecasts in time. The impact of tropical wind data in the forecasts of ultralong waves in the GLAS/NASA general circulation model has been documented by Baker and Paegle (1983). They obtained large differences in the tropical overturning motions between forecasts made with and without tropical wind data, suggesting the importance of heat driven circulations for global scale predictions. A follow up study (Paegle and Baker, 1983) examined the influence of tropical latent heating by comparing two simulations of the GLAS GCM started from the same initial conditions, one simulation used full physics and the other contained no latent heating in the tropical belt from 20° S to 20° N. Their main findings indicated the almost instantaneous (within a half day) impact of tropical heating in the divergent tropical motion while the rotational motions responded in about 3 and 5 days in tropical and

extratropical latitudes.

These and other studies have also pointed out difficulties in properly simulating tropical flows. This is probably due to the dominance of physical forcing in tropical latitudes, in contrast with mid-latitude flows which are more likely to be driven by flow instabilities and inertial effects. One primary source of energy in the tropics is the latent heat released in precipitation associated with active cumulus clouds (Holton, 1979).

Understanding of the physical processes which dominate in the tropics requires quantification of different components of the heat budgets from complete data sets for different seasons and time periods. The current research emphasizes the latent heat component in the tropical and subtropical region and its effect in the large scale overturning. The main goal is to quantify the time scale of these motions and their principal features as described by the heating rates obtained by GLAS/NASA and associated upper and lower level flow components.

1.2 Background

The Global Weather Experiment (GWE, December 1, 1978, November 30, 1979) provided unique data sets to understand this and other characteristics of the tropics. The most comprehensive program of atmospheric data acquisition ever attempted was successfully completed that year with strong international cooperation. Conventional observing systems were augmented utilizing newly developed techniques. Research data sets were compiled and archieved after careful checks to remove observational or processing errors. These

are denoted as level II-b or II-c data sets. The assimilation of such massive amounts of information presented a formidable challenge. Objective analysis methods were used to develop gridded fields using the level II data. These gridded fields are referred as level III-b sets and are now available from many operational centers and research institutes. These fields are somewhat dependent on the assimilation system used and it is therefore important to check the sensitivity of the results to the analysis methods.

For this study, the precipitation data gathered during this period (level II-c) are studied in conjunction with the GLAS heating fields and circulation data obtained from the III-b data sets. Partial comparisons of circulation statistics are presented using the European Center for Medium Range Weather Forecasting (ECMWF), Geophysical Fluid Dynamics Laboratory (GFDL), and Goddard Laboratory for Atmospheric Sciences (GLAS) analyses.

Daily values of precipitation data were gathered globally during 1979 directed to the second objective of the First GARP (Global Atmospheric Research Project) Global Experiment (FGGE): understanding of basic physical forces affecting climate. Data collected mainly as a result of this objective are referred to as level II-c sets. The global extent of this enhanced and checked precipitation data set is unique to the GWE year. It is therefore important not only to analyze this particular year, but also to compare it with more extensive climatologies whenever possible to isolate areas of averaged and anomalous atmospheric behavior. Such comparisons are also included in the present work.

CHAPTER 2

PROCEDURES

2.1 Data Acquisition

The following discussion describes analysis methods and data acquisition. The models used to obtain the heat and circulation fields are discussed. Heating rates, horizontal wind components, velocity potential, and stream function fields are studied and displayed in this research. Information about other fields is included in the discussion when necessary to complete the description of the physical phenomena of interest.

2.1.1 Precipitation Analyses

The precipitation data is from the FGGE data observed from December 1978 - November 1979. The unit is tenths of millimeters/ 24 hours and there are two categories of quality control: 1) accurate, checked, and found correct; 2) estimated, checked, and found correct. Category 2) is used to enhance the data set which otherwise would be very sparse in certain tropical areas. A trace of precipitation is equated to zero amount. Accumulating precipitation is averaged over the period and used for each day of the accumulating period.

Precipitation data are only available over land. This causes problems with analyses, contouring, and interpretation of global

tropical data, due to large oceanic areas void of data. Terrain features, such as mountain versus valley observation points, island location and topographic features, observation density, and other factors affect the reliability of the data. Future research needs to involve other available information such as satellite data, climatology, etc. to fill in data-sparse regions and increase reliability.

Recent developments in the use and interpretation of polar orbiter satellite data makes possible obtaining global representation of cloud cover, cloud top temperature, and pressure as well as surface temperature and vertical temperature and humidity profiles. The latter are routinely obtained by NOAA/NESDIS for operational purposes using the TIROS Operational Vertical Sounder (TOVS) system. Novel methods of combining radiance data with surface and atmospheric parameters (Susskind, et al., 1984) show promise for more accurate global determination of satellite-derived quantities and represent an alternative to methods based on statistical regression relationships. Another development measures water vapor over oceans. Microwave measurements of precipitating versus nonprecipitating clouds were derived by Hwang, et al. (1984) using the NIMBUS 7 Scanning Multichannel Microwave Radiometer (SMMR) data from December 1978 through November 1979. Satellite-derived precipitation values require further study before being used operationally. To be beneficial, procedures that obtain surface rainfall rates must first be developed.

Precipitation is highly variable depending on local terrain configuration and could attain very different values at points separated by short distances. Therefore only horizontally averaged

values are currently considered.

2.1.2 Heating Rate Fields

Estimated of diabatic heating fields can be obtained in one of three ways:

i) By direct evaluation of each component of the heating budget based on parameterization assumptions (e.g., Newell, et al., 1973). This method is highly dependent on the parameterization model used.

ii) As residuals of the thermodynamic energy equation. In this approach individual terms are evaluated from observed data (e.g., Luo and Yanai, 1984) or from gridded data (e.g., Murakami and Ding, 1982; Kasahara and Mizzi, 1983 using isobaric coordinates and Wei, et al., 1983 and Johnson, 1980 using isentropic coordinates).

iii) As residuals of the thermodynamic energy equation where individual terms are computed from either the first guess of objective analysis systems (e.g., Kalnay and Baker, 1984) or as forecasts in numerical integrations. In the case of assimilation systems which considerably weaken the tropical overturnings in the course of their initialization procedure, this method has the clear advantage of allowing the atmosphere to spin up in response to the model forcing.

A comparison of results obtained using method ii) by Kasahara and Mizzi (1983) and the GLAS heating rates obtained from the first guess analysis of their assimilation model (method iii)) was done Paegle and Paegle (1984).

Kasahara and Mizzi (1983) obtained the field as a residual of

the thermodynamic equations. The equation is:

$$\partial T/\partial t + \bar{V}\cdot\nabla T - w\Gamma = Q/C_p \qquad (2.1)$$

where $\Gamma = -(T/\theta)/\partial_\theta/\partial_p$ and Q/C_p = the residual heating/cooling rate. The $\bar{V}$ and T fields were analyzed every 6 or 12 hours. The resolution of this method was 1.875 x 1.875 degrees. The period of study was from January 27 - February 11, 1979. Its large scale features looked realistic, but they isolated two possible shortcomings: 1) A semi-diurnal wave #2 oscillation related to the divergence field was noted which may be caused by diurnal variation of cumulus convection, but was most probably due to different data density at 06 GMT; 2) Also, an over response in the mountainous areas was noted due to model divergence and vertical motion inadequacies in the vicinity of mountains.

The GLAS heating rates are evaluated in the course of the data assimilation using model diagnostics (method iii)). A damping time step is used for initialization to damp gravity waves, instead of the nonlinear normal mode initialization used by most operational centers. The model resolution is 4 degrees x 5 degrees and it has full physics. The thermodynamic equation used is:

$$\partial\theta_m/\partial t + \bar{V}_m\cdot\nabla\theta_m + W_m\cdot\partial\theta_m/\partial p = Q_m + \delta Q_{an} \qquad (2.2)$$

where m = model values and Q_{an} = the difference between the first guess and the analysis field. If the first guess was a perfect forecast, $\delta Q_{an} = 0$ and Q_m = the real atmospheric heating rates. Comparison of Q_m with those obtained by Kasahara and Mizzi (1983) for the

period January 27 - February 11, 1979 (Paegle and Paegle, 1984) showed that the heating rates from the model output: 1) did not have the unrealistic diurnal oscillations, and 2) were not as sensitive to the divergence analysis near the mountains as method ii). The GLAS heating fields appeared excessive in certain locations, though some computed peak heating rates of 10°C/day found for this period may be realistic. These values are likely to be observed in the tropics where the average value of precipitation is 2 cm of precipitation releasing approximately 5°C/day of heat over a column of atmosphere (Holton, 1979).

2.1.3 Circulation Diagnostics

The circulation variables have been computed from three different data sets, obtained by ECMWF, GFDL, and GLAS/NASA. Further comparison of results obtained from different assimilation methods is desirable to quantify the sensitivity of conclusions to the analysis scheme. No heating rates were available from the GFDL and ECMWF assimilation cycles, so the intercomparisons are limited to: U and V wind components, velocity potential, and stream function fields.

The GLAS FGGE III-b data set used a successive correction method which included weights depending on the data quality and density for the analysis scheme (Baker, 1983). The analysis and forecast system used the GLAS 4th order GCM (Kalnay and Baker, 1984) with a damping time step during initialization as previously indicated and included all diabatic processes. The available analyzed fields included horizontal wind components, temperature, humidity, and sea level pressure. Also, sensible and latent heat, precipitation, and total

diabatic heat fields were produced and archived.

The ECMWF III-b data set used intermittent data assimilation and a nonlinear normal mode initialization (Bengtsson, 1983). The analysis was performed in pressure coordinates while the forecast was carried out in a high resolution sigma coordinate system. Its analyzed fields of geopotential heights, sea level pressure, and horizontal wind fields were not initialized; whereas, the derived fields of temperature, relative humidities, and vertical velocities were initialized. The data are available in isobaric surfaces with values interpolated under the surface in mountainous areas. The vertical velocities are too weak as a result of the nonlinear normal mode initialization (Carr and Ramamurthy, 1983; and Lambert, 1983). These resulted in reduction of the mean meridional circulation and wind divergence in the tropics. Another possible problem was the pronounced diurnal cycle of the tropical divergence field. In fact, the 06 GMT divergence was nearly one half the values at 00 GMT and 12 GMT in certain regions. This may be partly due to data gaps in the cloud track winds at 06 GMT which may be obscuring an actual atmospheric response (Paegle, 1983; and Julian, 1983).

All models used the 6 hour forecast fields as the first guess to analyze new data. The analyses should mostly reflect observations in regions of high data density and model forecasts in data sparse regions where more of the model's first guess was used. The Geophysical Fluid Dynamics Laboratory (GFDL) Level III-b data sets used a continuous dynamic assimilation system and a nonlinear normal mode initialization. The model was a global spectral GCM. The first guess was the most recent analysis, with weights assigned for

accuracy and interpolation to fill in gaps. Also, the model results versus analysis were weighted depending on reliability of the data. As time progressed real observed data were inserted into the model, so that the data and the model's dynamics and physics were consistent. Virtues of the model were consistency among variables and the control of error growth. Problems were data rejection and the noisy appearance of the model (Stern and Ploshay, 1983). Also, the model underestimated severe storm patterns at times and its vertical velocities were exceedingly noisy in the tropics (Miyokada, et al., 1983).

When comparing the ECMWF products to the GFDL model, the GFDL products had shallower troughs, stronger divergent flows, and stronger return flows in the Hadley Circulation (Stern and Ploshay, 1983).

2.2 Analysis Methods

The following discussion focuses on the format of the precipitation, heat, and circulation fields, along with some problems involving these quantities.

2.2.1 Precipitation Analysis

Precipitation data are only available over land. Observed values may vary greatly within short distances due to regional effects. Therefore only horizontally averaged data over either 1 7/8° x 1 7/8° grid size or 4° x 5° grid are used in this study. These grid intervals are chosen to agree with those of GFDL, ECMWF, and GLAS analyses.

The analysis covers different averaging periods. Periods

covered are seasonal, weekly, and daily.

Typical station distributions and data coverage for the precipitation fields are shown in Figures 2.1 - 2.5. Maximum number of stations, using Figure 2.4, is found in the densely populated areas of Australia and Southeast Asia. In those regions the observation counts are 1792, 420, and 224 for grid areas centered at eastcentral Australia, Malaysia, and the Philippines, respectively. The Hawaiian Islands contribute about 350 observations per grid point while at the maritime region of Indonesia about 10 observations per grid point are found.

Figures 2.6 and 2.7 display averaged precipitation amounts. Each grid point value includes all reporting stations that have acceptable quality control values. A look at the seasonal and weekly graphs shows that the 4° x 5° grid loses a lot of detail. It also reduces the maximum amounts by averaging the precipitation over a larger area. Largest precipitation rates of 3.5 cm/day are found during the summer season in conjunction with the Asian monsoon in the higher resolution grid. This maximum is lowered to 2.2 cm/day in the 4° x 5° grid. The week of January 5 - 11 displays a remarkably active South Pacific Convergence Zone with precipitation amounts of about 6 cm/day over the Pacific Ocean and 5.2 cm/day over northeastern Australia. These patterns are greatly distorted in the 4° x 5° grid (Figure 2.5), with only the Australian maximum apparent in the analysis. It is therefore preferable to use the 1 7/8° x 1 7/8° grid to display the precipitation amounts. This is done in the next chapter.

The station density for each grid varies as seen in the

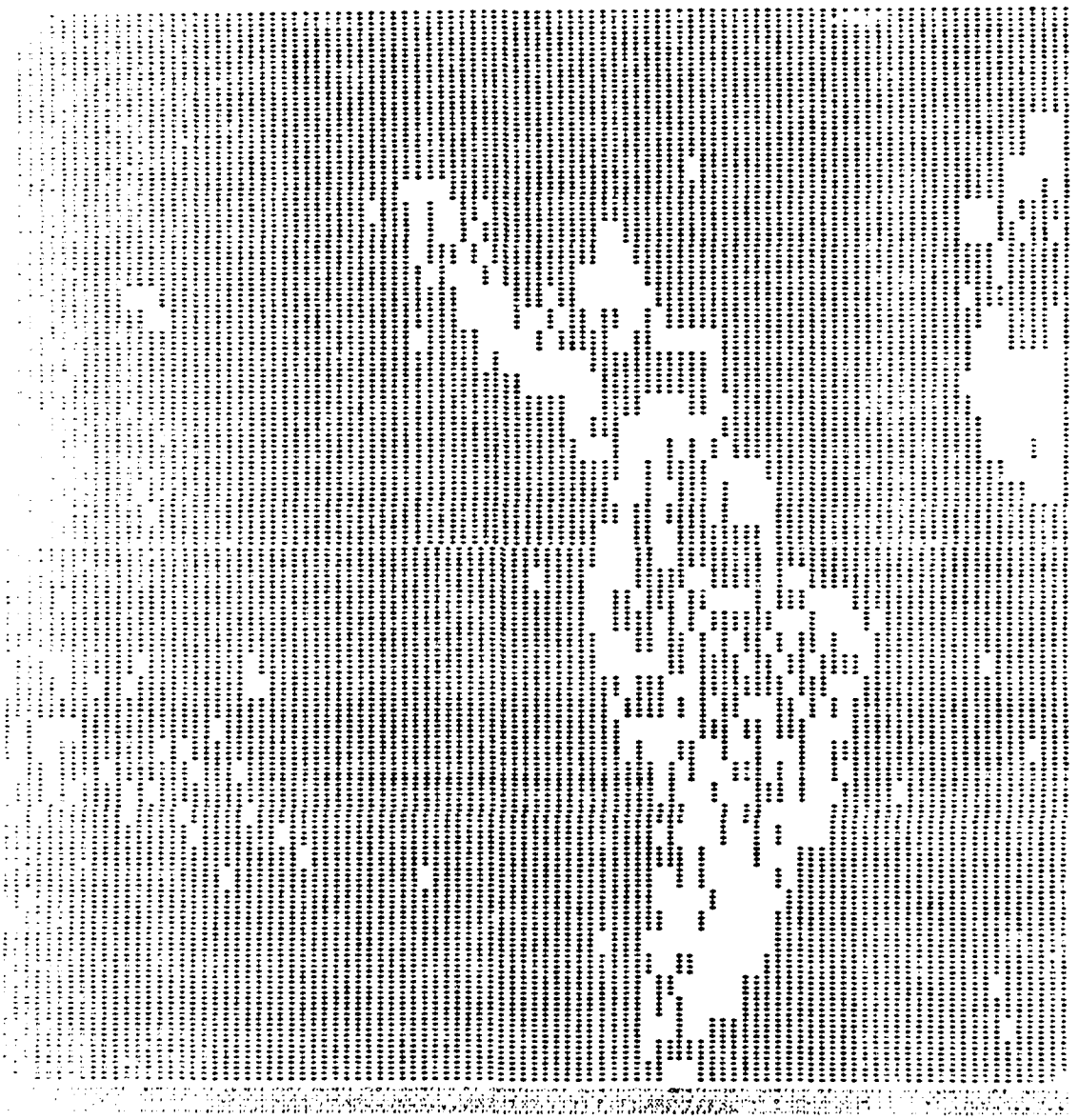

Figure 2.1. Continued.

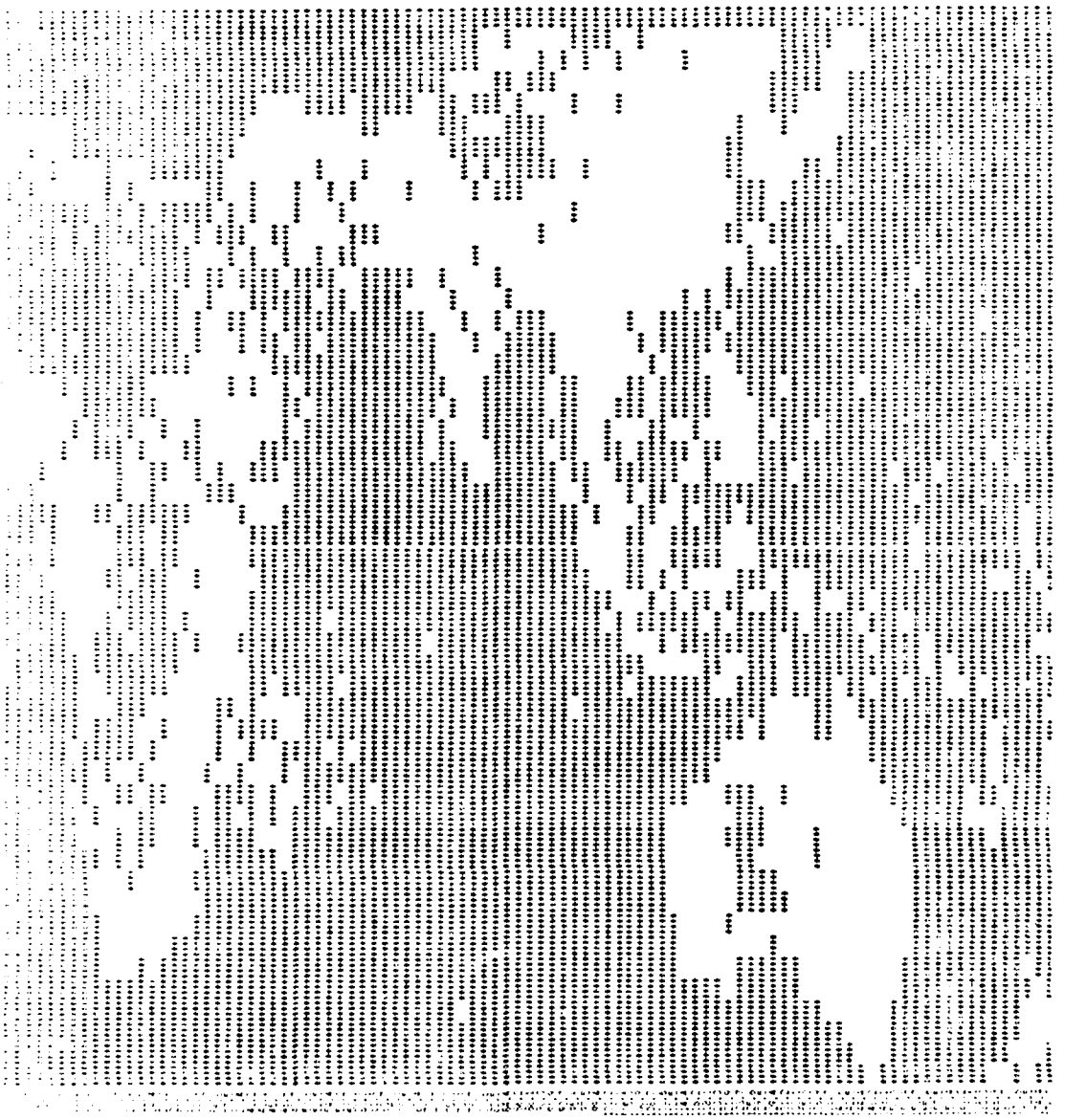

Figure 2.1. Locations of FGGE precipitation data (blank areas) on 1 7/8° x 1 7/8° grid of world.

Figure 2.2. Locations of FGGE precipitation data (blank areas) on 4° x 5° grid of world.

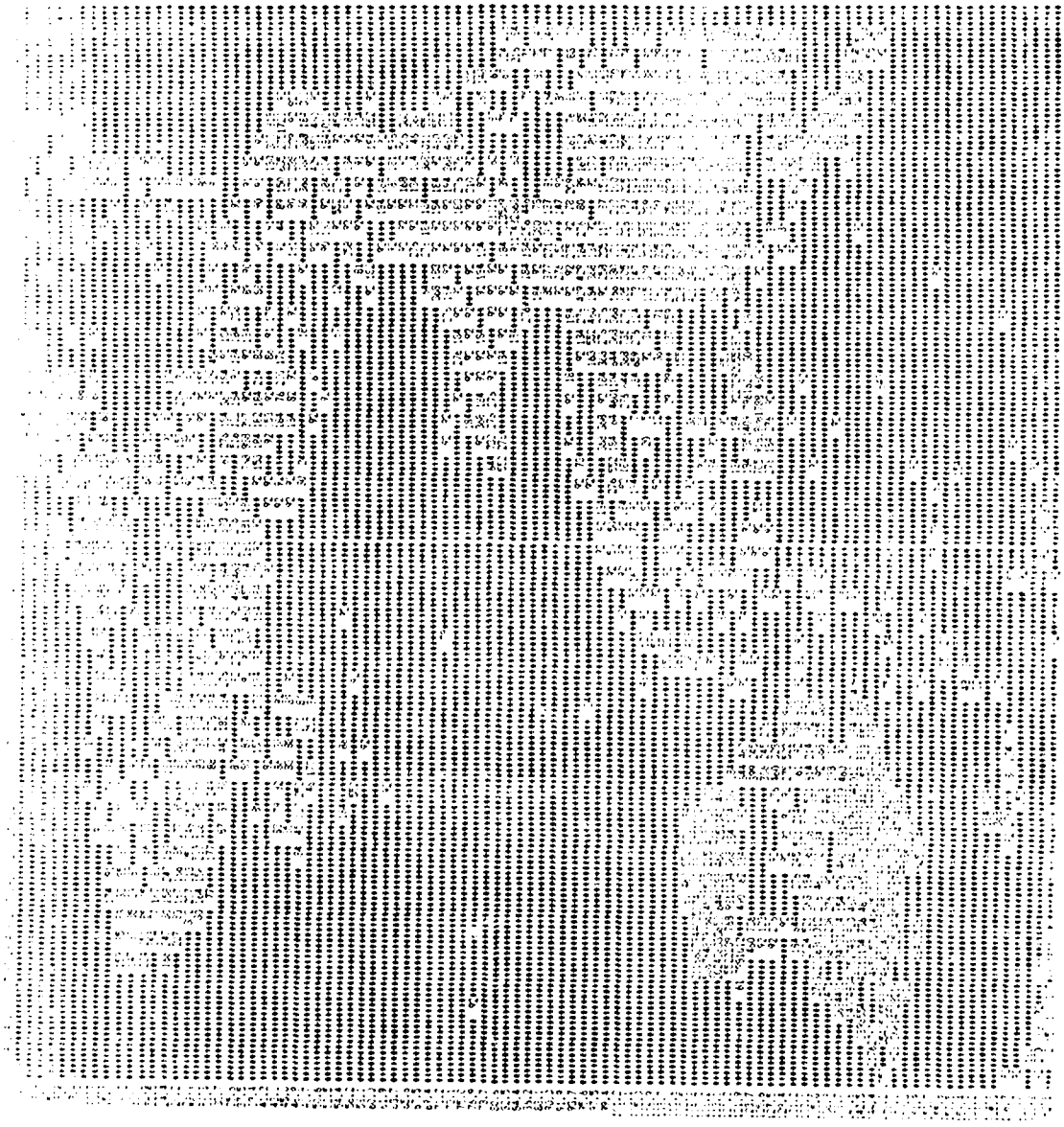

Figure 2.3. Seasonal station count for 1 7/8° x 1 7/8° gridpoints.

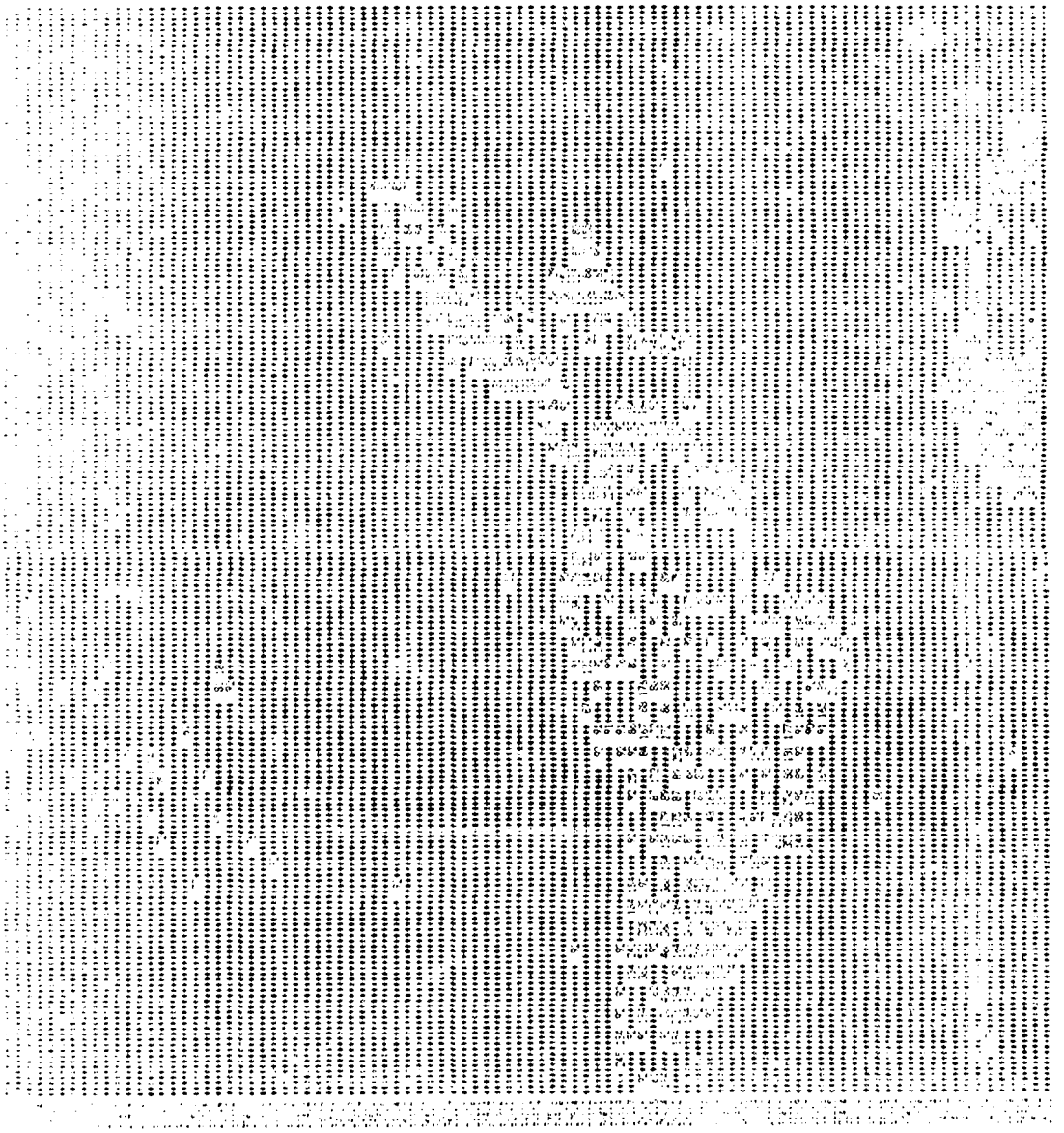

Figure 2.3. Continued.

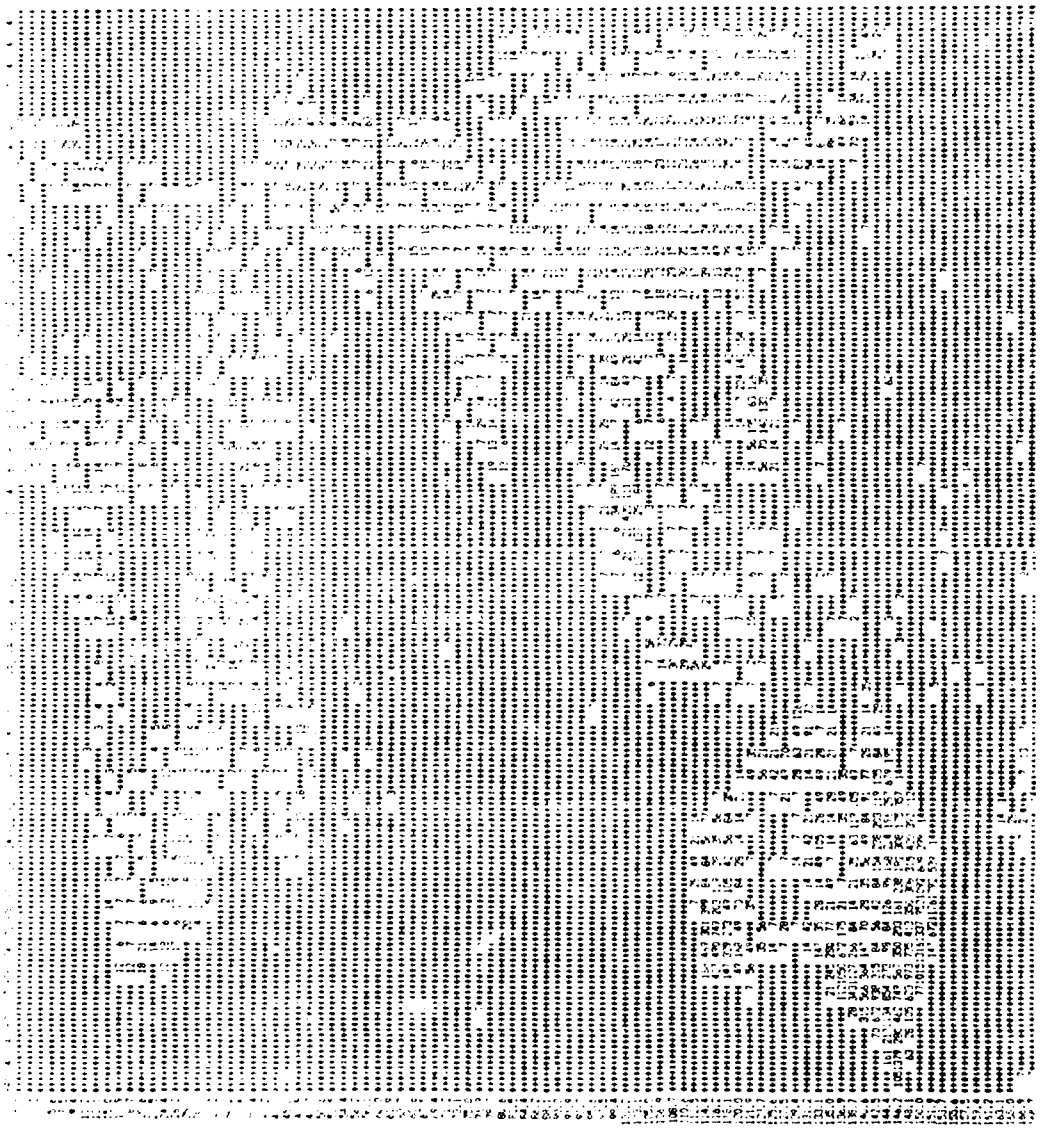

Figure 2.4. Weekly station count for 1 7/8° x 1 7/8° gridpoints.

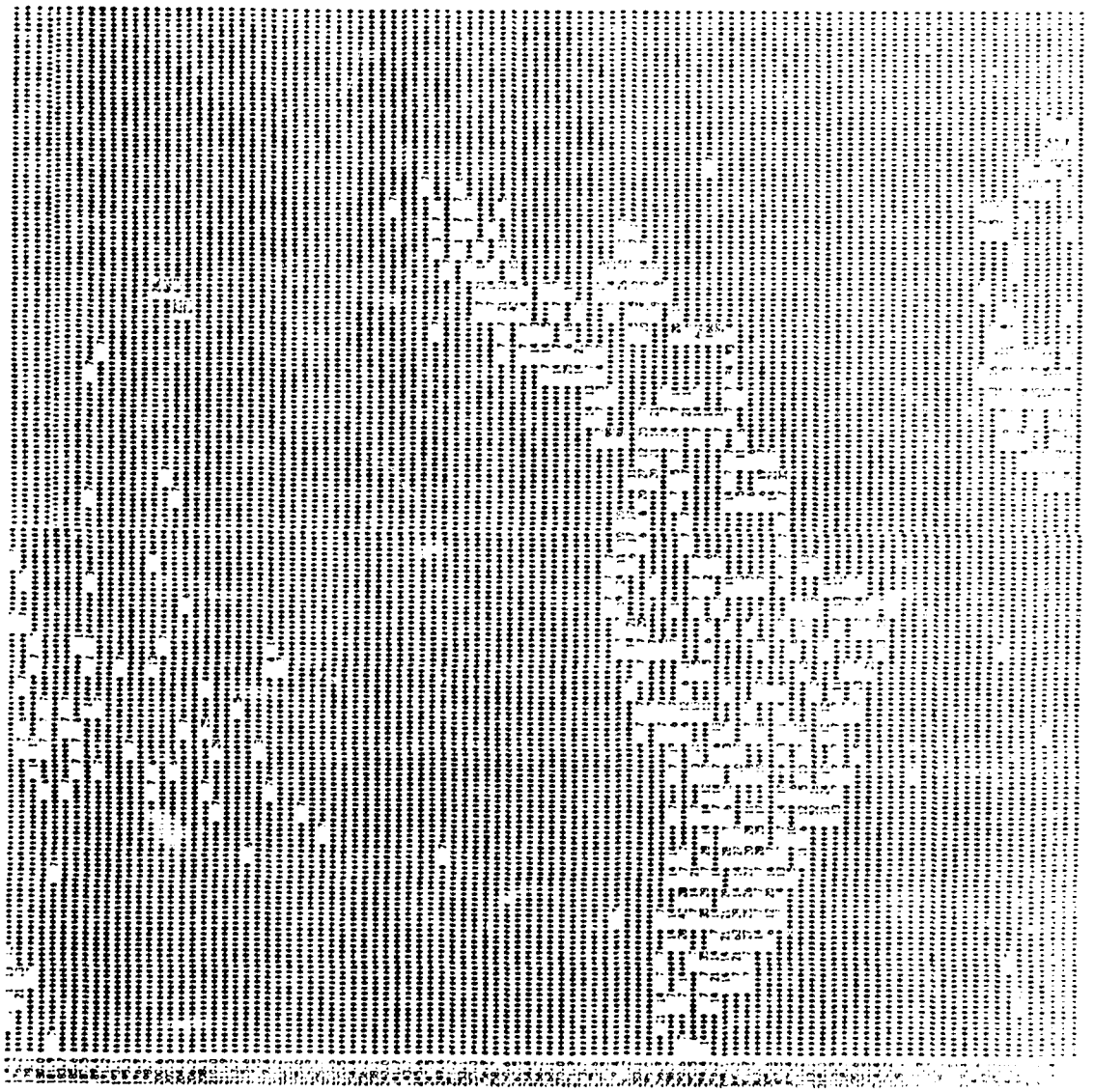

Figure 2.4. Continued.

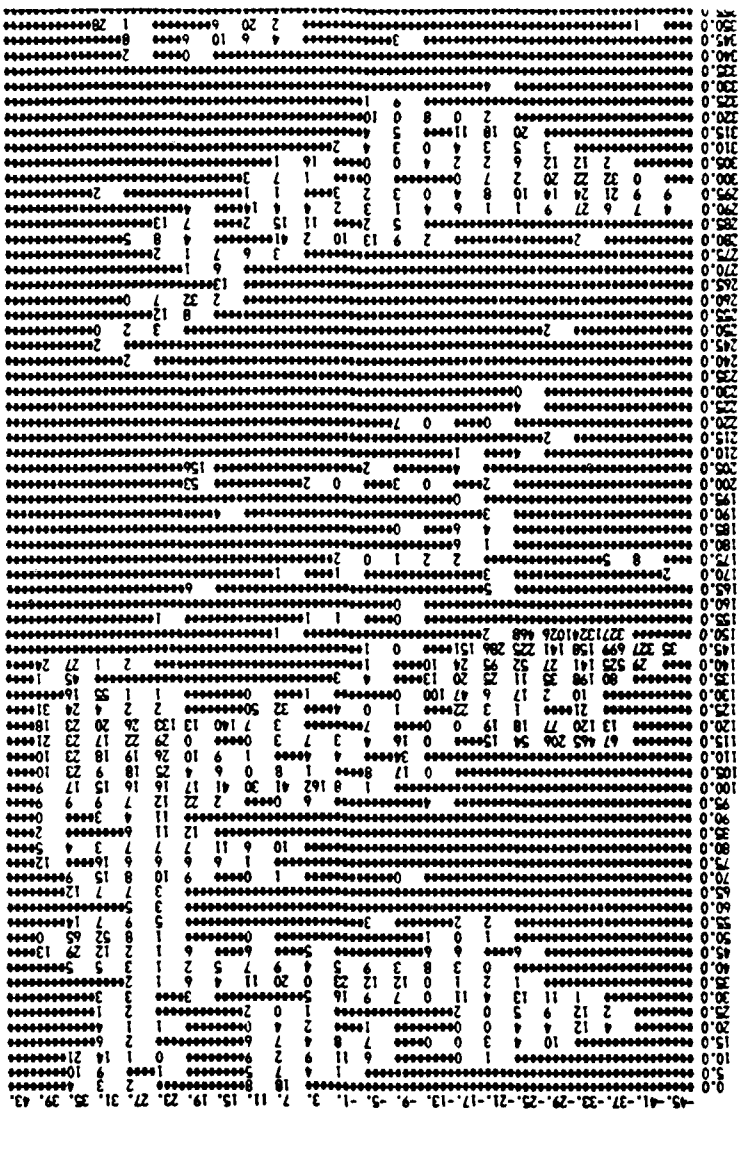

Figure 2.5. Weekly station count averaged for 4° x 5° gridpoints.

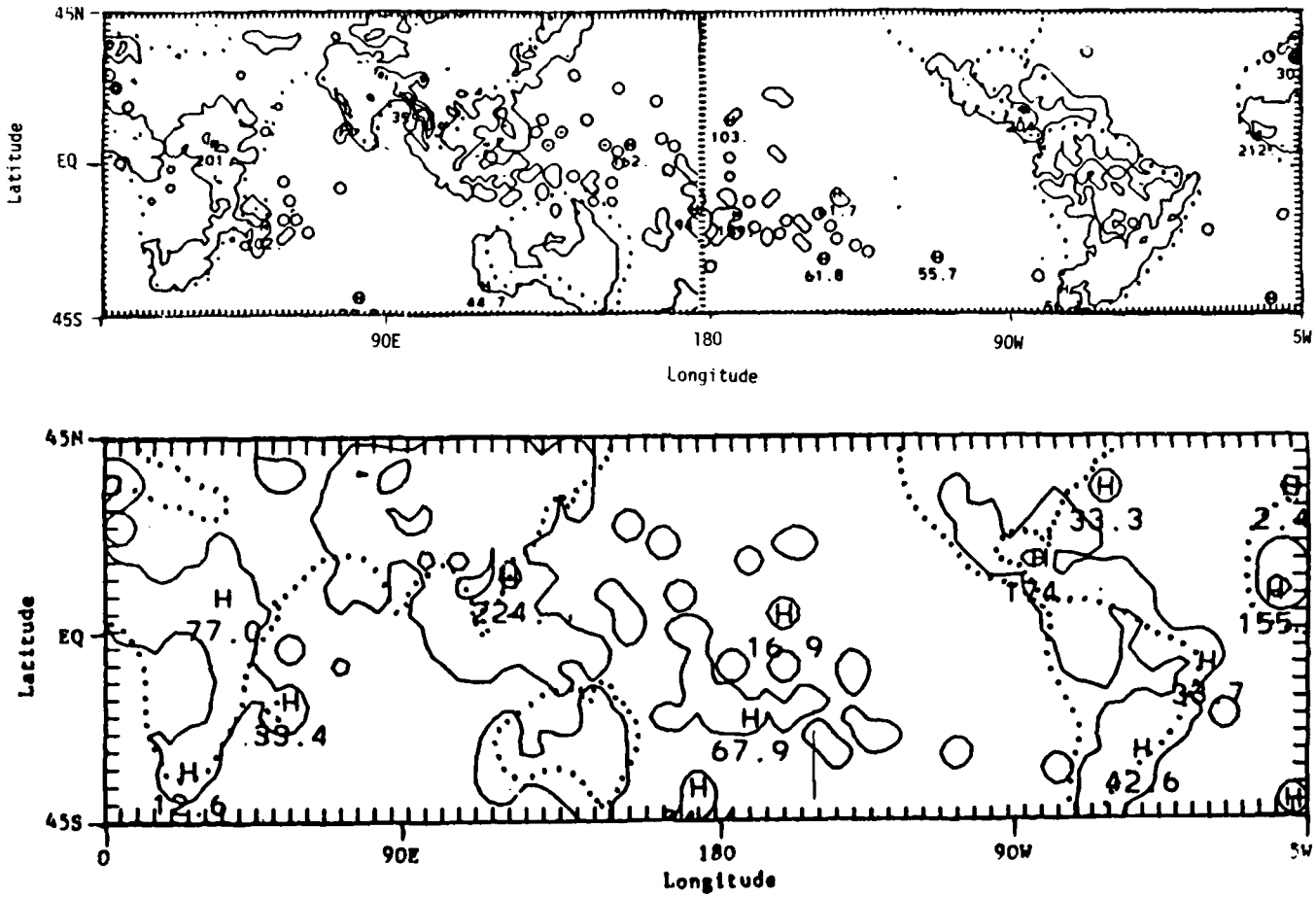

Figure 2.6. Averaged precipitation amounts, June - August 1979, contour interval of 100.0 x 10^{-1} mm/day. Units are tenths of mm/day.
(a) 1 7/8° x 1 7/8° grid
(b) 4° x 5° grid

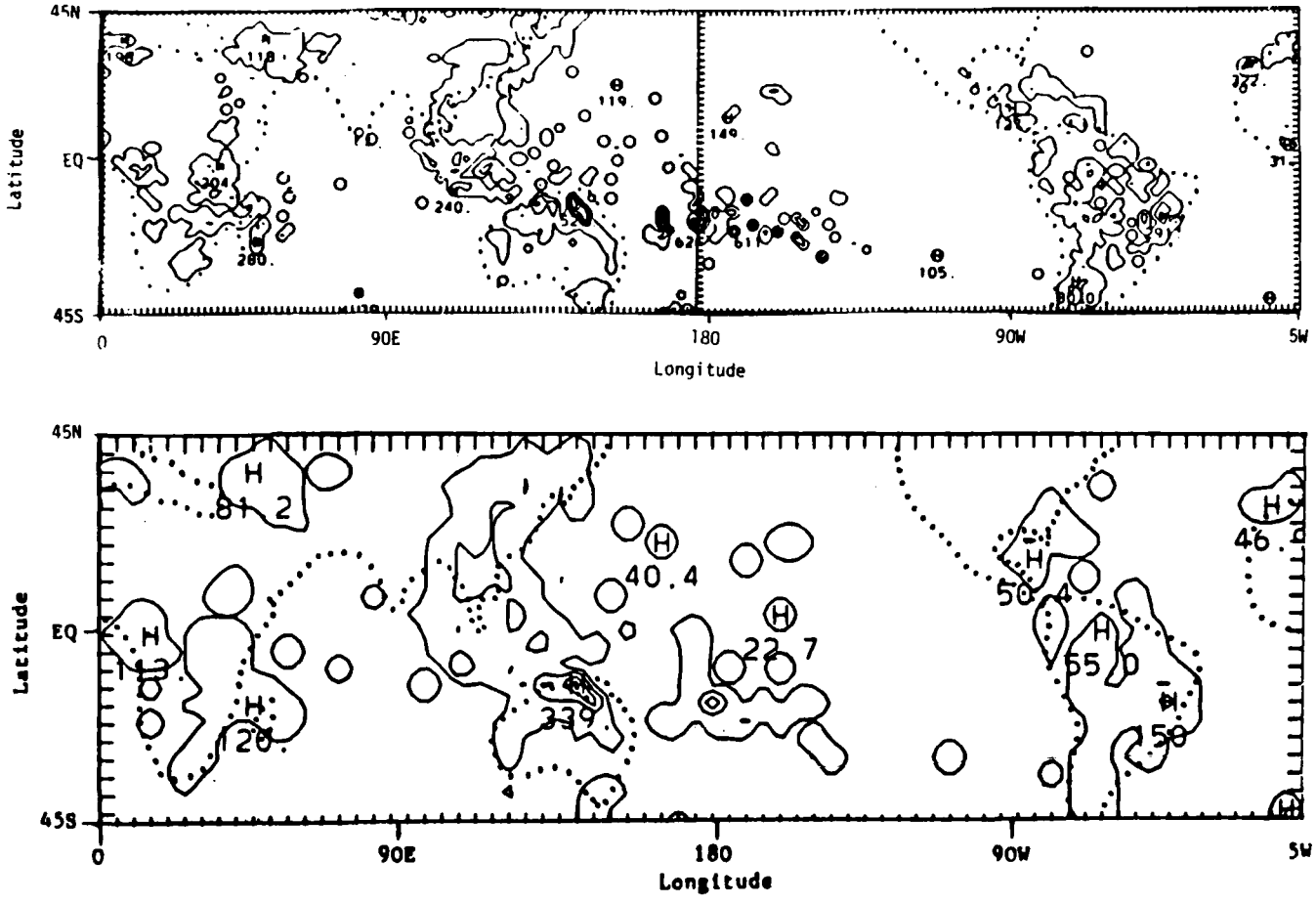

Figure 2.7. Averaged precipitation amounts, 5 January - 11 January, 1979, contour interval of 100.0 x 10^{-1} mm/day. Units are tenths of mm/day.
(a) 1 7/8 x 1 7/8° grid
(b) 4° x 5° grid

station count figures mentioned above. The computer programs read the data, perform any needed calculations, average values for each grid point, and arrange the individual grid values into a world map.

2.2.2 Heating Rate Analysis

Heating rates were derived by GLAS/NASA using the methods described in the Data Acquisition section presented above. Grid point values are available in the GLAS 4° x 5° analysis grid at 9 sigma levels. This field includes latent heating, sensible heating, solar radiation, and infrared cooling. The latent heat release is of particular interest to this study for comparison with precipitation data.

The heating fields obtained from GLAS are vertically integrated and averaged over different periods. Discussion will center on seasonal, weekly, and daily values.

The programs read the values derived by the GLAS model, perform vertical averages, and arrange the individual grid values into a world map similar to that obtained for the precipitation fields.

2.2.3 Circulation Analysis

FGGE level III-b data sets from ECMWF and GFDL are available in 1 7/8° by 1 7/8° (latitude, longitude) grid as mentioned above. U and V gridded fields are interpolated to a 4° by 5° (latitude, longitude) grid for comparison with the GLAS data sets. A two dimensional linear interpolation scheme is used for this purpose.

Vorticity (ζ) and divergence (δ) are computed for each data set at several vertical levels. The Poisson equations used are:

$$\nabla^2 \psi = \zeta \tag{2.3}$$

$$\nabla^2 \chi = \delta \, . \tag{2.4}$$

They are numerically solved over the whole globe to obtain the stream function (ψ) and velocity potential (χ). The method proposed by Paegle and Tomlinson (1975) is used for this purpose.

The following chapter presents circulation statistics for the 200 and 850 mb levels.

CHAPTER 3

RESULTS

3.1 Introduction

The main features of the global tropical circulations may be inferred from available climatologies (e.g., Newell, et al., 1973). Tropical latitudes provide a large amount of the energy needed to maintain atmospheric circulations against frictional dissipation. Sensible and latent heat are transported at lower levels equatorward and are lifted and condensed in preferred tropical regions, producing potential energy and sensible heat. Upper level circulations transport this energy poleward. Condensation processes are of great importance in this process and are the central theme of the current investigation.

It is not a simple task to infer the characteristics of overturnings from conventional data. Since precipitation data present a number of limitations already discussed, it is desirable to obtain heating rate estimates from other methods. The current research uses the heating rates derived at GLAS/NASA and compares them with precipitation data for cross validation. These comparisons are done for a variety of time and horizontal scales: 1) Seasonal comparisons between FGGE data and climatological charts for precipitation, heating rates, and U and V wind components are presented; 2) Weekly averages are contrasted for the two special observing periods of

January 5 - March 1, 1979 and May 12 - August 3, 1979; 3) Heating and velocity potential data are presented at 00, 06, 12, and 18 GMT for the week of January 5 - 11, 1979; 4) Daily variations of precipitation are compared with mid atmosphere heating rate variations for selected area averages from January 5, 1979 to February 28, 1979.

3.2 Seasonal Averages

The FGGE year is likely to remain the most complete atmospheric data sets for the tropics and the Southern Hemisphere for many years. It is important therefore to document the differences observed with respect to more extended climatologies to assess whether atypical atmospheric behavior during 1979 is due to i) the enhanced data sets, or ii) time variations in short climatic scales (of the order of .1 to 10 years). Once anomalous atmospheric characteristics are isolated extensive research is needed to determine whether they are due to i) or ii) above. For example, Trenberth and van Loon (1981) and Trenberth (1984) have discussed the rather anomalous behavior of the Southern Hemisphere during FGGE. In particular during the months of April to July 1979, they found abnormally low sea level pressures over the Southern Hemisphere (high pressure over the Northern Hemisphere). On the other hand, Karoly, et al. (1983) attribute the deep values of the circumpolar Southern Hemisphere lows to the extended network of floating buoys deployed during the FGGE. The discussion in the present work will concentrate on latitudes from 45° orth to 45° south.

The seasonal precipitation averages display a typical trend of maximum precipitation in the Southern Hemisphere during the December

through February season (Figure 3.1) and in the Northern Hemisphere during the June through August season (Figure 3.2). The transition periods, March - May and September - November, are shown in Figures 3.1 and 3.2.

The FGGE values are compared with the climatology presented in volume one and two of the book by Newell, et al. (1973). In general, the dry and wet areas tend to match up between the FGGE data and the climatological data. Anomalously high precipitation values are found over Morocco, Cape York (Australia), and Madagascar during the winter season. During the summer, the maximum precipitation values are almost twice as strong as those found in the extended climatology.

The winter season presents maximum values over Madagascar, Indonesia, over the northeastern Australian penninsula of Cape York, the South Pacific Convergence Zone (SPCZ), and the Amazon basin. A northward shift of maximum precipitation values is clearly apparent as the year progresses. During the summer season the strongest precipitation values are associated with the Asian monsoon, with the maximum precipitation rates located over Central America in the Western Hemisphere.

The winter seasonal precipitation is now compared to the winter heating field displayed in Figure 3.3. There is a general correspondence of higher rainfall with higher heating rates over the Amazon basin and Indonesia. Precipitation maxima over Madagascar, the SPCZ (at about 15 degrees south and the dateline), and northeastern Australia have no counterpart in the heating fields. A strong heating maxima of 12.6°C/day over the equatorial regions of

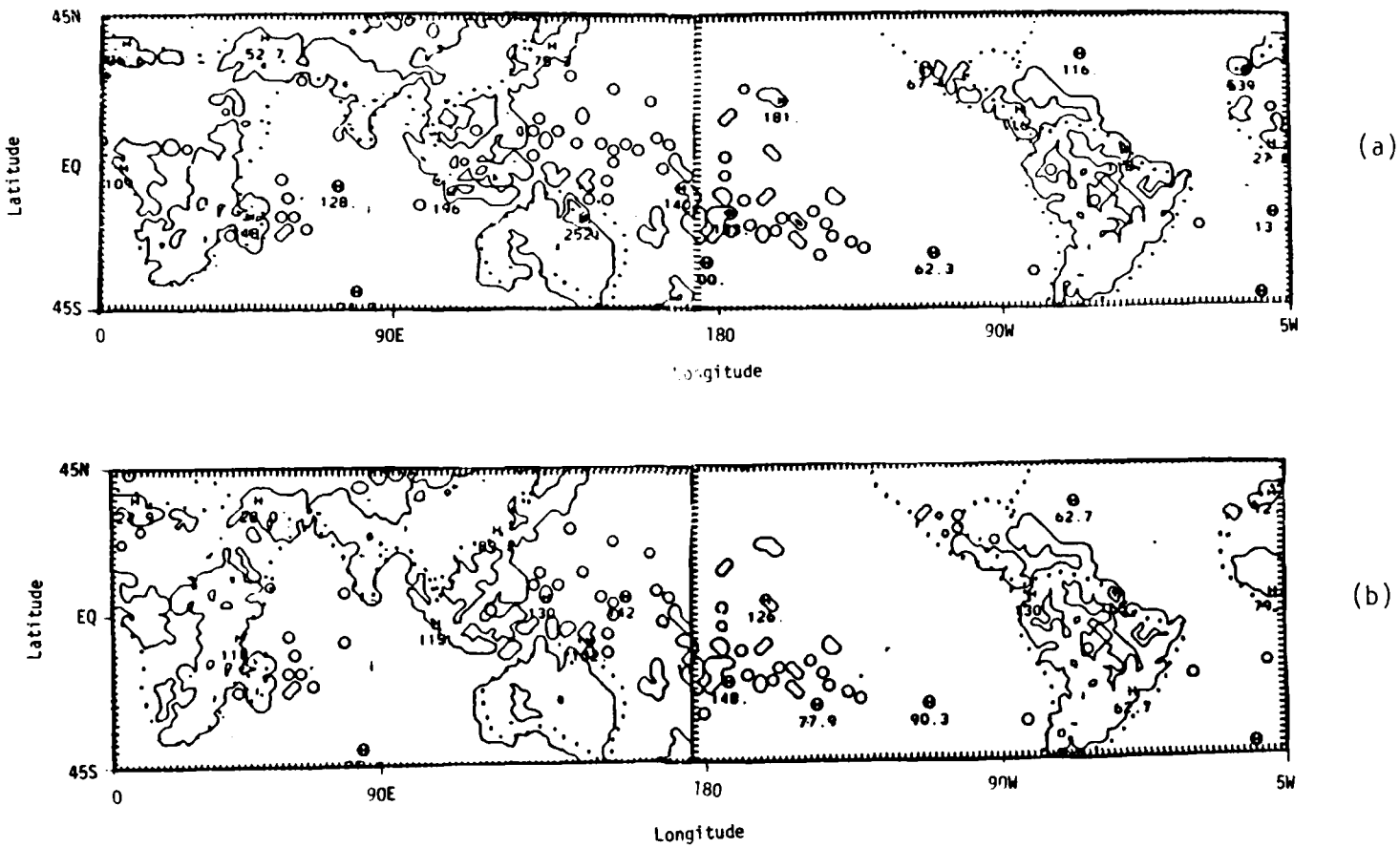

Figure 3.1. Averaged precipitation amounts, 1 7/8° x 1 7/8° grid, contour interval of 100.0 x 10^{-1} mm/day. Units are tenths of mm/day, December to May, 1979.

(a) December 1978 - February 1979

(b) March - May, 1979

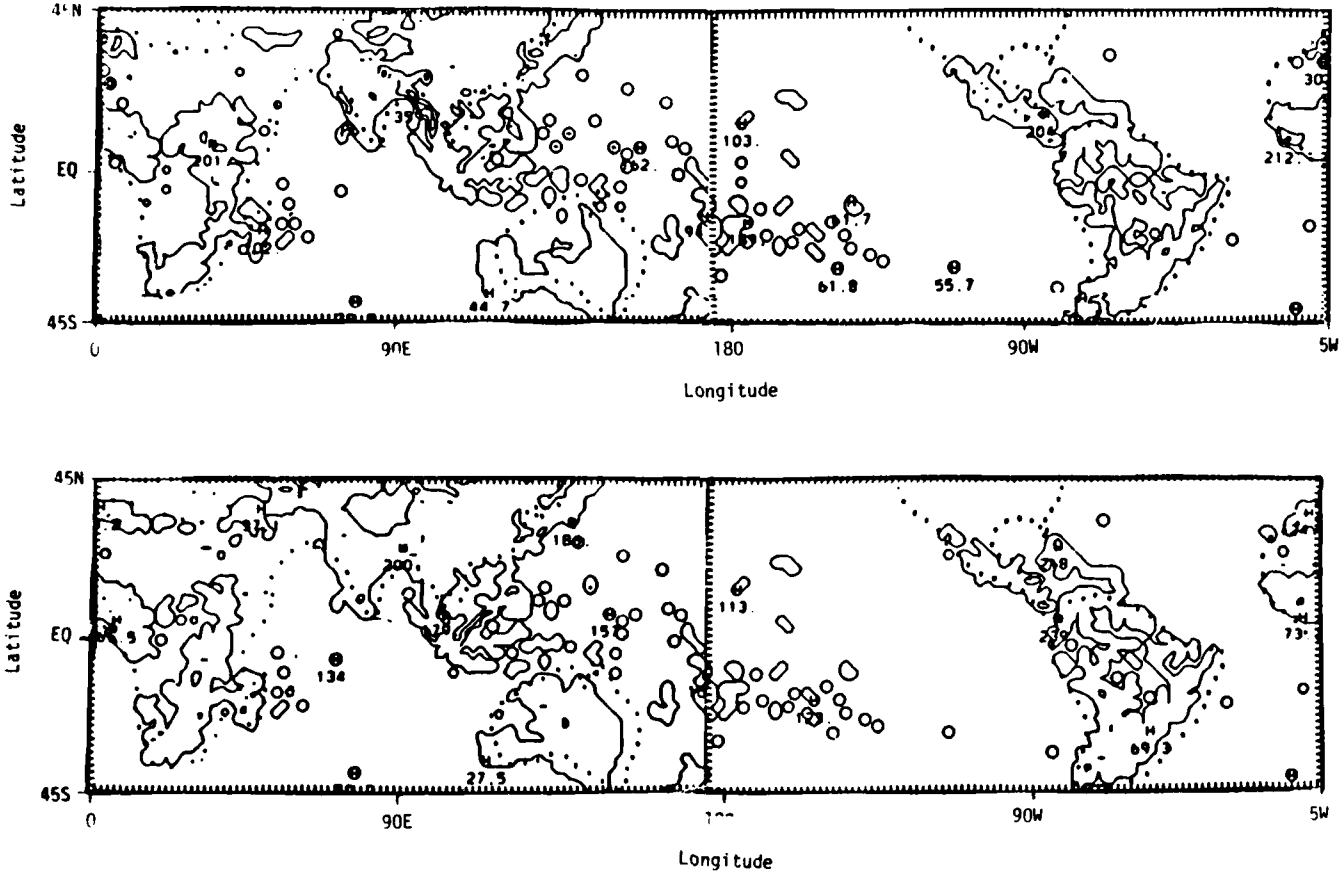

Figure 3.2. Averaged precipitation amounts, 1 7/8° x 1 7/8° grid, contour interval of 100.0 x 10^{-1} mm/day. Units are tenths of mm/day, June to November, 1979.

(a) June - August, 1979

(b) September - November, 1979

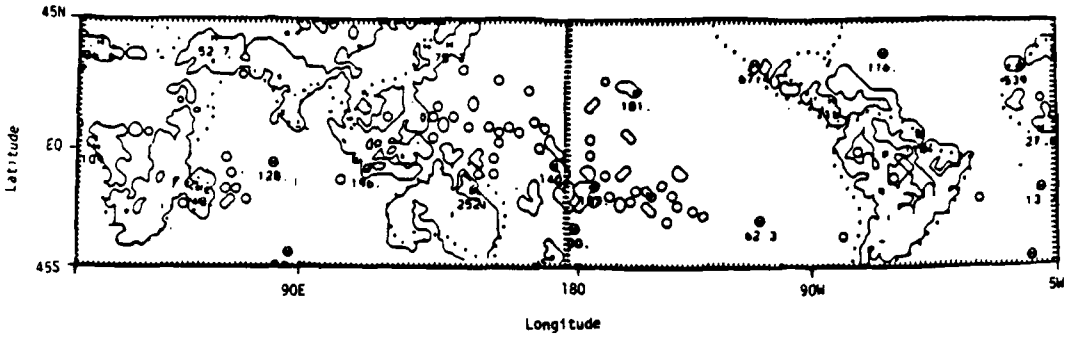

(a)

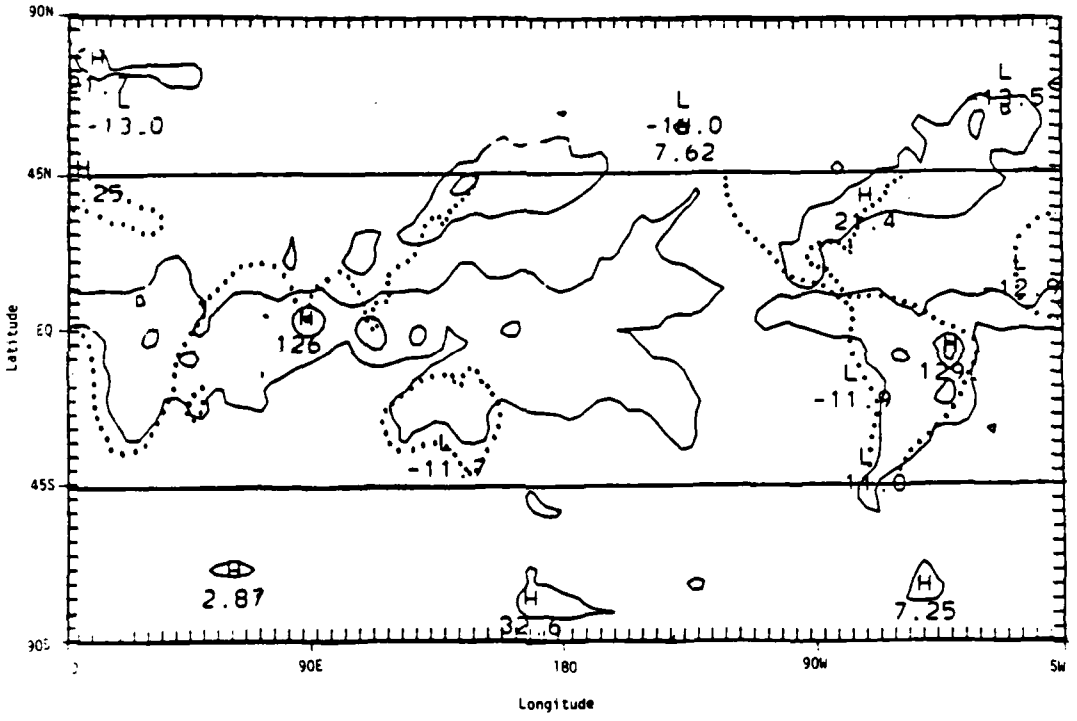

(b)

Figure 3.3. Precipitation and heating rates.
(a) Averaged precipitation amounts, December 1978 - February 1979, 1 7/8° x 1 7/8° grid, contour interval of 100.0 x 10^{-1} mm/day. Units are tenths of mm/day.
(b) Column integrated heating rates averaged for 5 January - 1 March, 1979 ((00Z + 12Z)/2), contour interval of 50.0 x 10^{-1}°C/day. Units are tenths of degrees Centigrade/day.

the Bay of Bengal is present in a region with no available precipitation data. Heating fields include sensible heat, solar radiation, and infrared besides latent heating in the analyzed fields. The heating rates look to be too low over Australia and Northwest Africa and too high over the Amazon basin of South America. This possibly can be attributed to the land cover (Trewartha, 1968). Over Australia and Northwest Africa the land surface has more of a desert type vegetation and a greater degree of outgoing radiation, whereas the Amazon has tropical vegetation and less radiation escaping back into the atmosphere (Petterssen, 1969). Therefore, comparisons of the vertical integrated heat fields with precipitation data must be done with caution.

The winter season U and V (Figure 3.4) components are also compared to the climatological charts of both components of the wind velocity. Main differences between the FGGE year and the more extended climatology are: 1) The absence of a separate westerly maxima over the Arabian penninsula and South America during FGGE; 2) A stronger jet east of Australia and a well-developed westerly maximum south of Africa during FGGE. Both features are found about 15 degrees south of their climatological location; 3) The meridional motions associated with the convective tropical regions of the Southern Hemisphere are in general stronger during FGGE, with northward flows about 50% higher and a southerly maximum displayed over Melanesia of about 9 m/s not present in the more extended climatologies.

Paegle, et al. (1983) compared the global wind distributions of the FGGE and Data System Test (DST) for the summer of 1976. Their

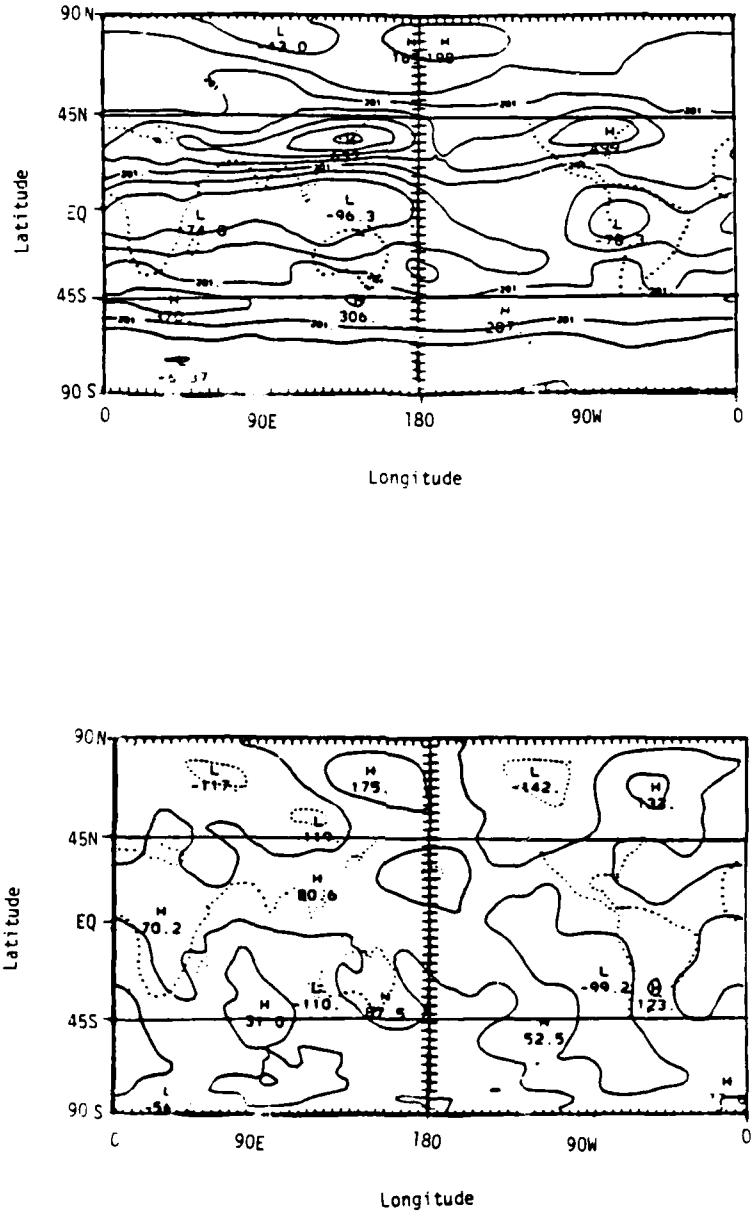

Figure 3.4. Averaged components of 200 mb wind, 5 January - 1 March, 1979, contour interval of 100.0 x 10^{-1} m/sec. Units are 10^{-1} m/sec.
(a) U component
(b) V component

results show stronger westerly jets over Australia and South Africa for the FGGE than for the DST year. Similar conclusions are reached when the FGGE year is compared to the more extended climatology of Newell, et al. (1973). These stronger circulations may be related to the Southern Hemisphere anomalies previously mentioned.

3.3 Weekly Averages

Considerable interest has been evoked during the last decade on low frequency oscillations with 30 to 50 day periods. These have been detected as eastward propagating disturbances in the tropical sea level presure field (Madden and Julian, 1971, 1972) and eastward propagating planetary divergence waves (Lorenc, 1984). Meridionally propagating low frequency weather systems found by Krishnamurti and Subrahmanyam (1982), especially over the Asian monsoon region, were related to cloud cover by Yasunari (1980, 1981) and to active and inactive spells of the Asian monsoon by Sikka and Gadgil (1980). Krishnamurti, et al. (1984) noted a strong relatinship between the passage of the divergence wave and wet and dry spells of the monsoon region. The dependence of these disturbances on tropical convection and divergence patterns makes their study directly relevant to our current research.

These phenomena are best studied by filtering atmospheric data to isolate the periods of interest as done, for example, by Krishnamurti and Gadgil (1984). In this section weekly averages are presented which effectively remove disturbances with short (less than 7 days) time scales.

Results are obtained for 8 weeks in the winter and 12 weeks in the summer, but only a smaller subset of representative charts are

shown.

The precipitation and heating fields are shown in Figures 3.5 through 3.11 for the first, fourth, and seventh week of the first Special Observing Period (SOP-1) and for the second, fifth, tenth, and twelfth week of the Second Observing Period (SOP-2). These weeks are selected to display the various precipitation regimes found for different weeks. The precipitation and heating fields show an overall trend of increased precipitation corresponding to areas of higher heating rates. This is especially noticeable when winter and summer weeks are contrasted. As the highest areas of precipitation move from the Southern Hemisphere in the winter to the Northern Hemisphere in the summer months, so do the heating fields. This is also a response to the incoming radiation flux moving to the Northern Hemisphere as the seasons progress from winter to summer.

The first week in SOP-1 is characterized by a very active South Pacific Convergence Zone with values up to 6 cm/day observed in equatorial latitudes close to the dateline. Three weeks later the maximum heating rates are found over the Indian Ocean, rainfall of 8 cm/day are reported over the northeastern coast of Australia, while precipitation has markedly decreased over the dateline. Maximum values are found again close to the dateline 3 weeks later. These features will be related to circulation characteristics below.

The strongest summer precipitation values are found for the twelfth week of SOP-2 with values of 8 cm/day over India. The one week averages for May and June (Figures 3.8 and 3.9) on the pre-onset phase of the Asian monsoon, display typical precipitation maxima over southeast China, Burma, and the Bay of Bengal. After

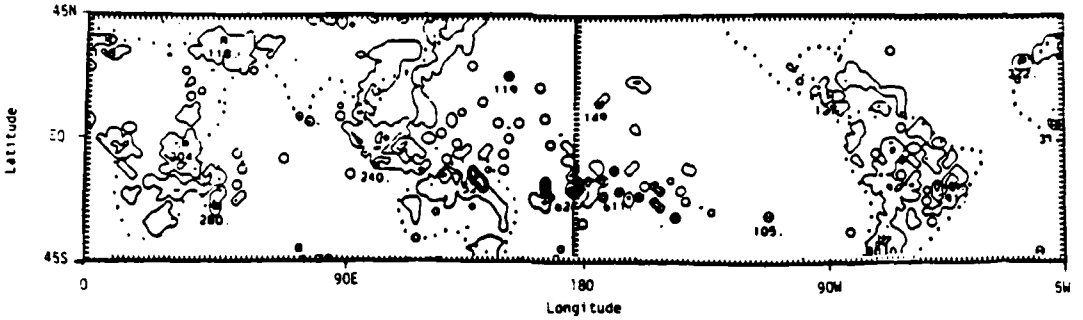

(a)

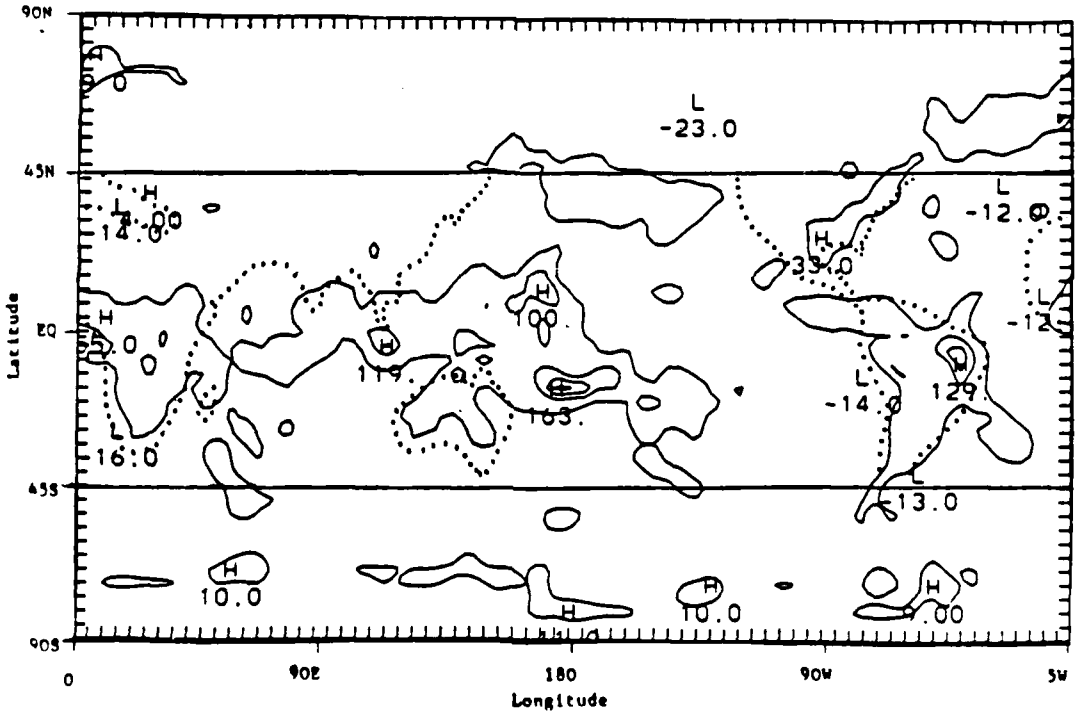

(b)

Figure 3.5. Precipitation and heating rates for 5 January - 11 January, 1979.

(a) Averaged precipitation amounts, 1 7/8° x 1 7/8° grid, contour interval of 100.0 x 10^{-1} mm/day. Units are tenths of mm/day.

(b) Averaged column integrated heating rates ((00Z + 12Z)/2), contour interval of 50.0 x 10^{-1}°C/day. Units are tenths of degrees Centigrade/day.

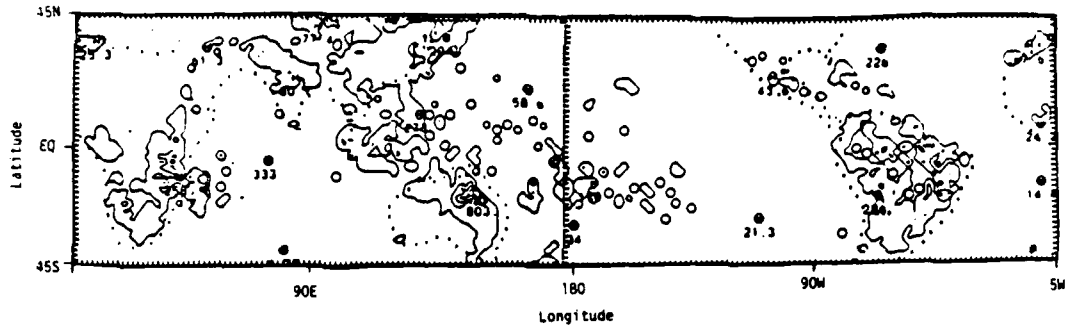

(a)

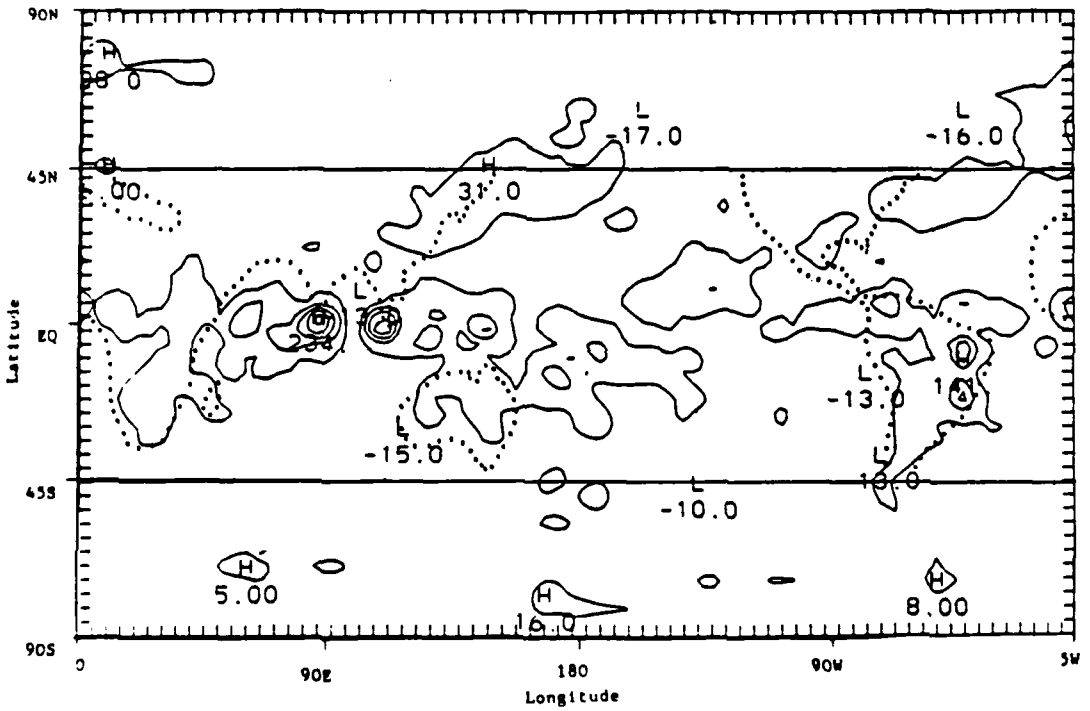

(b)

Figure 3.6. Precipitation and heating rates for 26 January - 1 February, 1979.

(a) Averaged precipitation amounts, 1 7/8° x 1 7/8° grid, contour interval of 100.0 x 10^{-1} mm/day. Units are tenths of mm/day.

(b) Averaged column integrated heating rates ((00Z + 12Z)/2), contour interval of 50.0 x 10^{-1}°C/day. Units are tenths of degrees Centigrade/day.

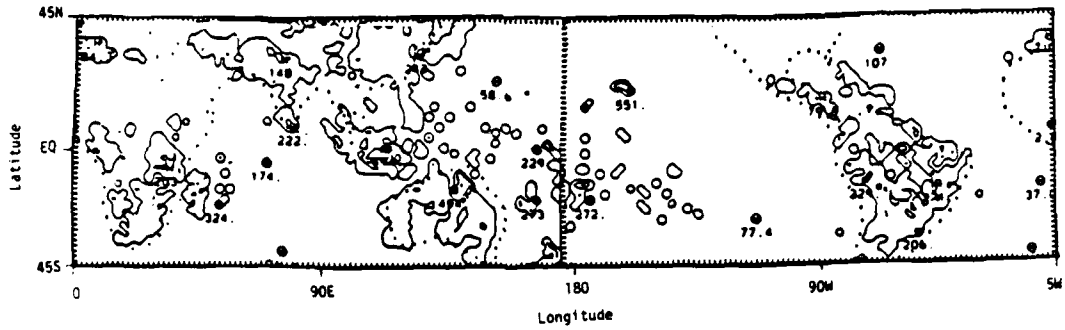

(a)

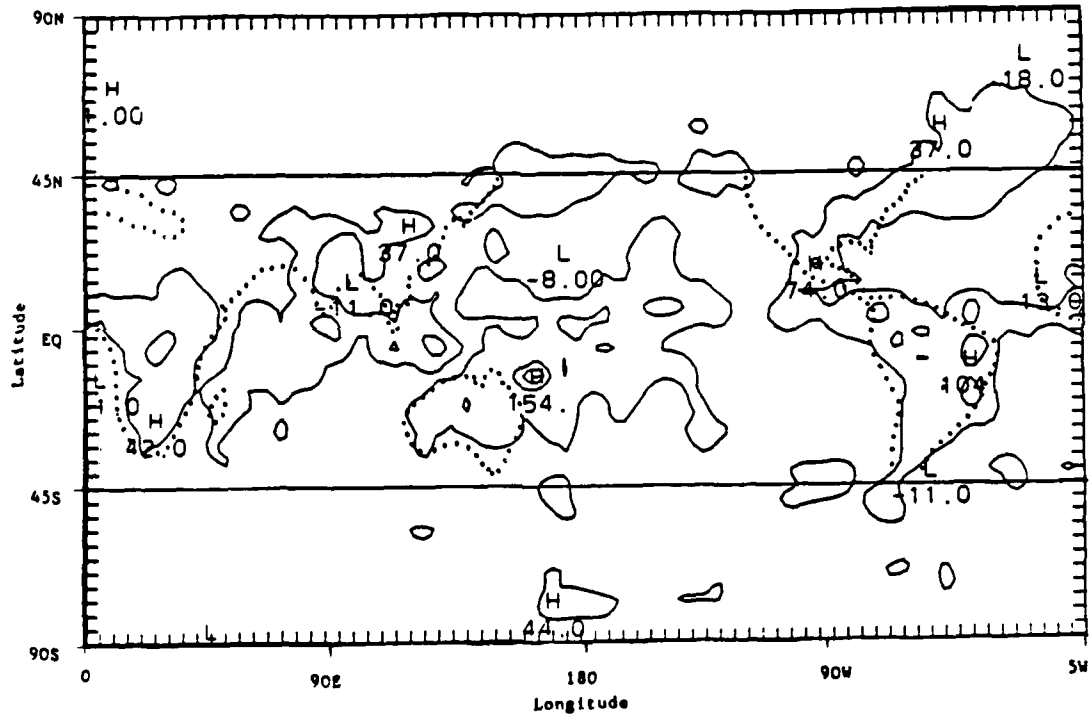

(b)

Figure 3.7. Precipitation and heating rates for 16 February - 22 February, 1979.

(a) Averaged precipitation amounts, 1 7/8° x 1 7/8° grid, contour interval of 100.0 x 10^{-1} mm/day. Units are tenths of mm/day.

(b) Averaged column integrated heating rates ((00Z + 12Z)/d), contour interval of 50.0 x 10^{-1}°C/day. Units are tenths of degrees Centigrade/day.

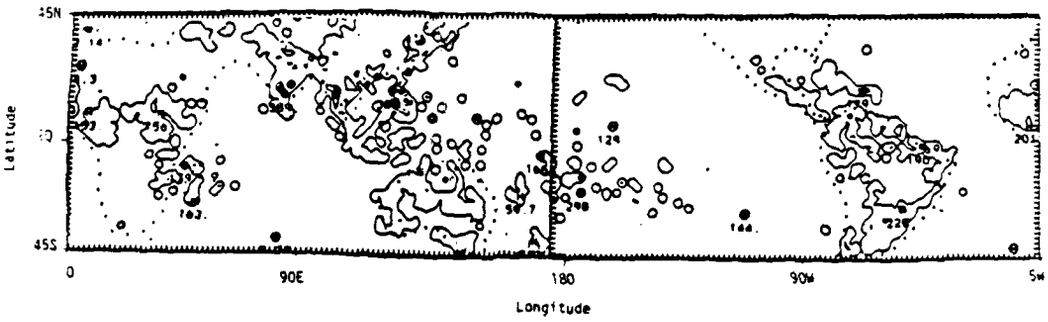

(a)

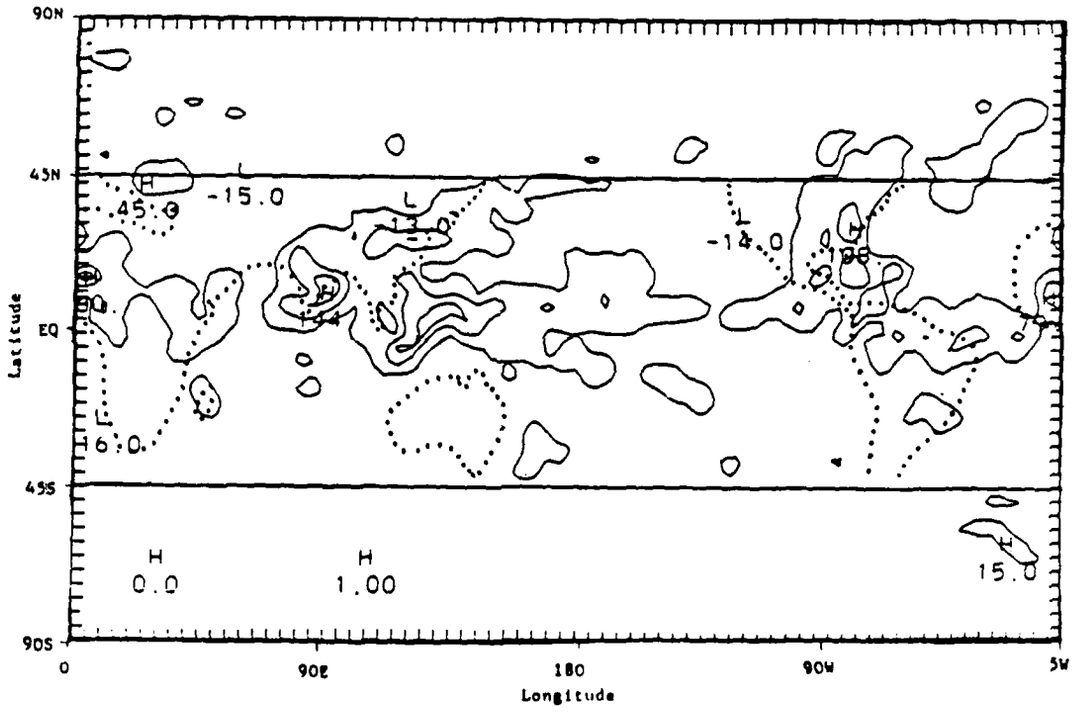

(b)

Figure 3.8. Precipitation and heating rates for 12 May - 18 May, 1979.

(a) Averaged precipitation amounts, 1 7/8° x 1 7/8° grid, contour interval of 100.0 x 10^{-1} mm/day. Units are tenths of mm/day.

(b) Averaged column integrated heating rates ((100Z + 12Z/2), contour interval of 50.0 x 10^{-1}°C/day. Units are tenths of degrees Centigrade/day.

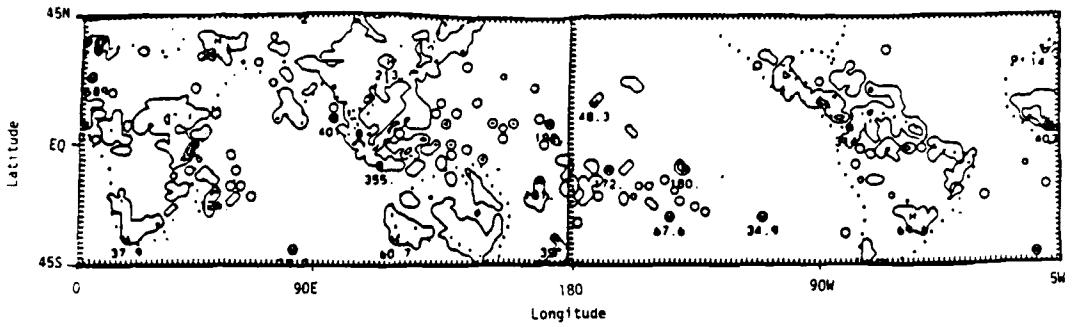

(a)

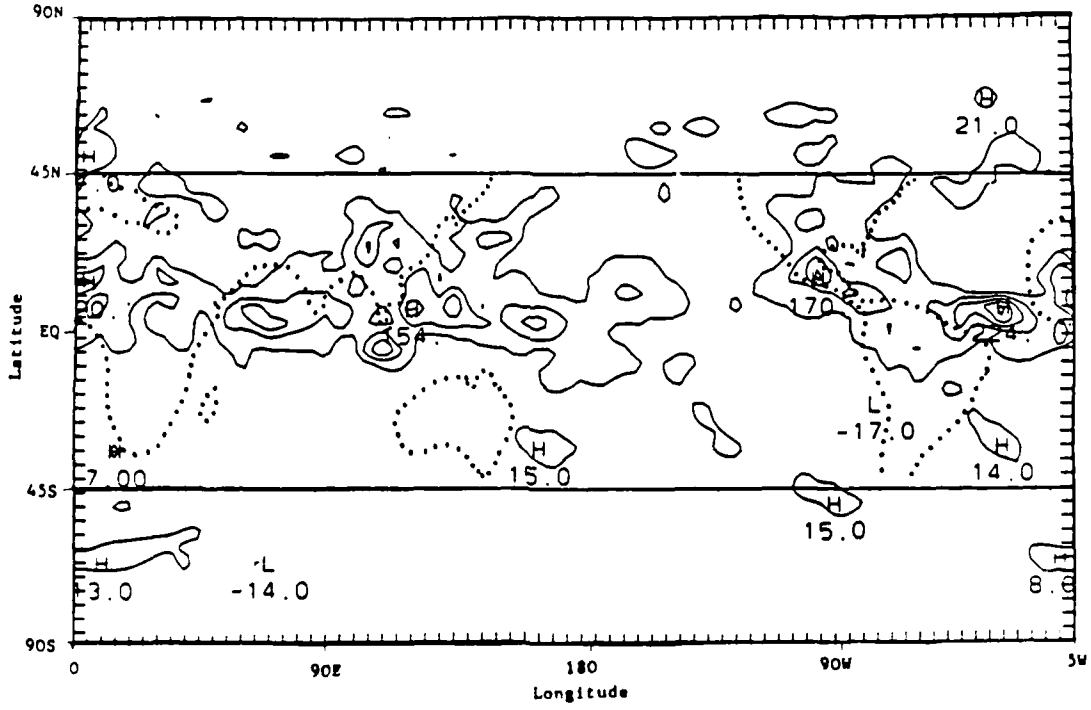

(b)

Figure 3.9. Precipitation and heating rates for 2 June - 8 June, 1979.

(a) Averaged precipitation amounts, 1 7/8° x 1 7/8° grid, contour interval of 100.0 x 10^{-1} mm/day. Units are tenths of mm/day.

(b) Averaged column integrated heating rates ((00Z + 12Z)/2), contour interval of 50.0 x 10^{-1}°C/day. Units are tenths of degrees Centigrade/day.

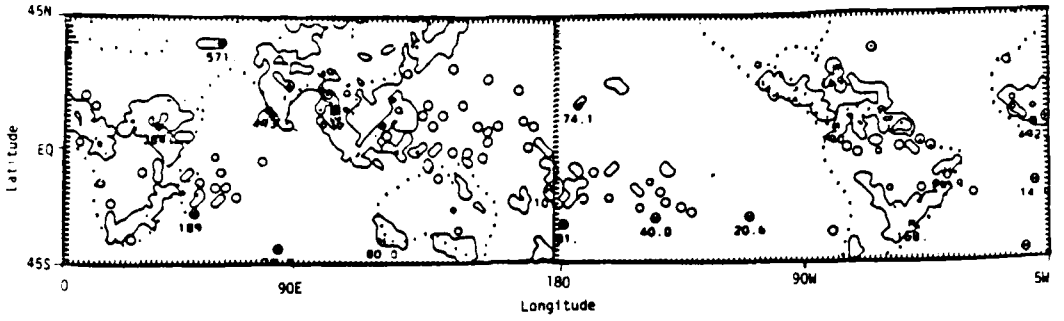

(a)

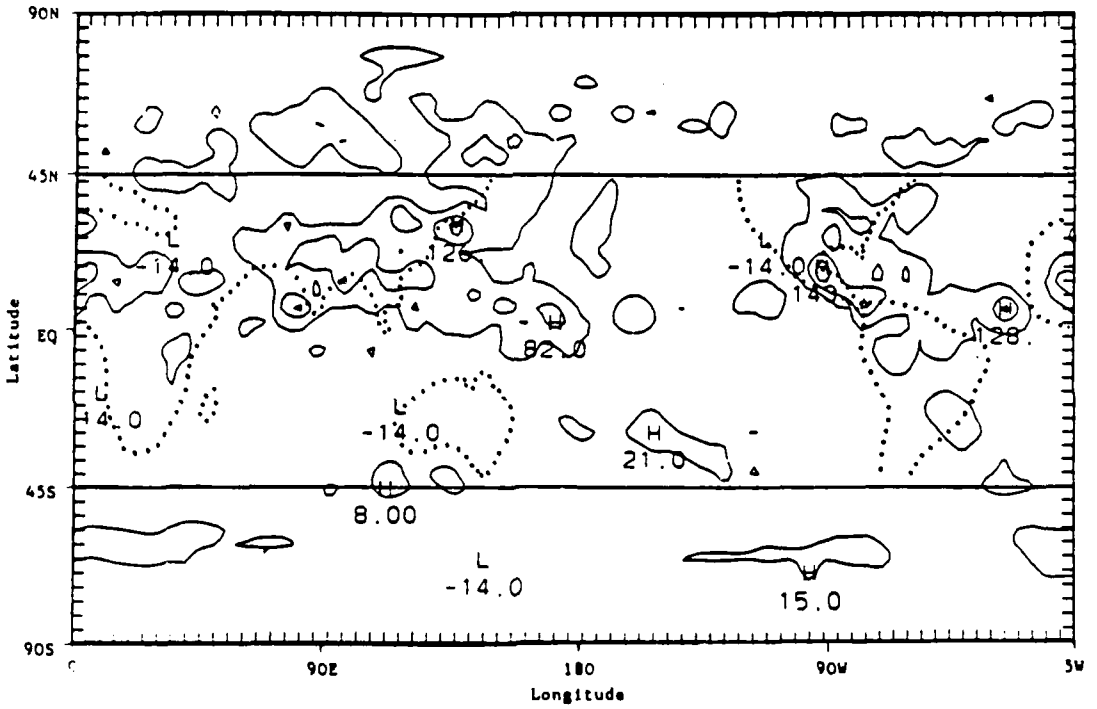

(b)

Figure 3.10. Precipitation and heating rates for 7 July - 13 July, 1979.

(a) Averaged precipitation amounts, 1 7/8° x 1 7/8° grid, contour interval of 100.0 x 10^{-1} mm/day. Units are tenths of mm/day.

(b) Averaged column integrated heating rates ((00Z + 12Z)/2), contour interval of 50.0 x 10^{-1}°C/day. Units are tenths of degrees Centigrade/day.

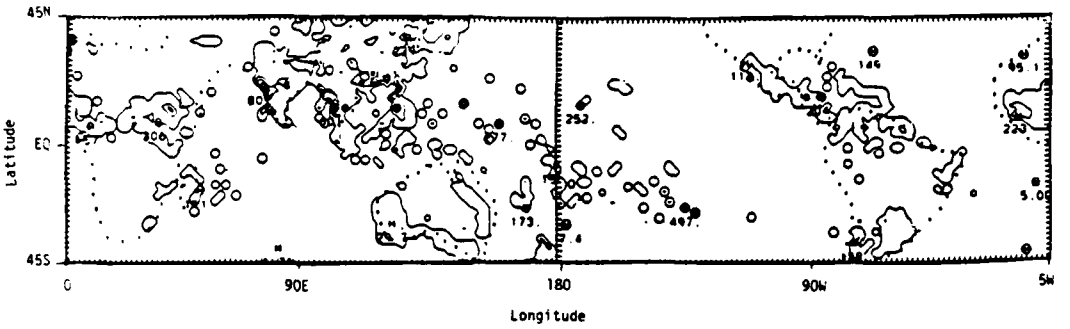

(a)

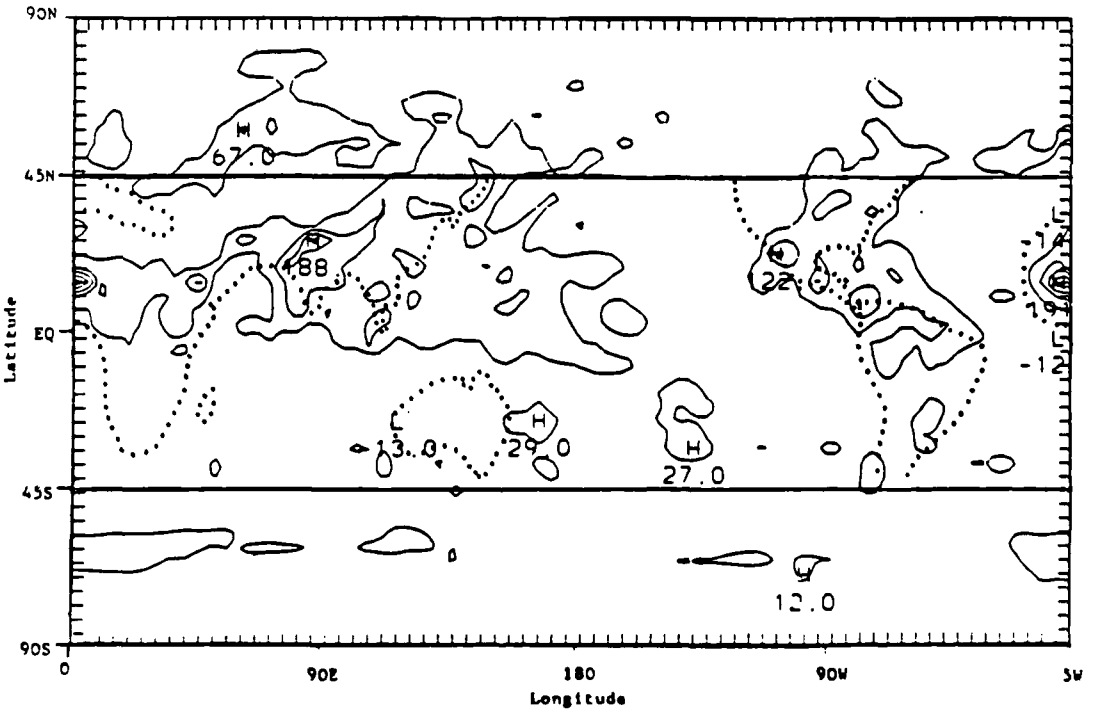

(b)

Figure 3.11. Precipitation and heating rates for 28 July - 3 August, 1979.

(a) Averaged precipitation amounts 1 7/8° x 1 7/8° grid, contour interval of 100.0 x 10^{-1} mm/day. Units are tenths of mm/day.

(b) Averaged column integrated heating rates ((00Z + 12Z/2), contour interval of 50.0 x 10^{-1}°C/day. Units are tenths of degrees Centigrade/day.

June 18 the Asian summer monsoon of 1979 was fully established. Heavy rainfalls are recorded over India from this date on, with intermittent wet and dry spells. These features are more closely seen in Figures 3.12 through 3.14 which show the week averages subtracted from the SOP-1 and SOP-2 averages.

High precipitation rates over Australia in the winter time have no counterparts in the heating rates. Also, over South America the high heating rates do not have as high precipitation values as other areas of comparable high heating rates. The Australian differences could be due to the lack of thick vegetation and corresponding greater radiational cooling. Over South America, high precipitation values may be missed by the sparsity of the reporting precipitation network. This is especially true over vast ocean areas where at times there are not data. The Indian Ocean maxima could not be validated with precipitation data due to the lack of stations in this area.

Velocity potential and stream function weekly averages as well as their differences from seasonal averages are shown in Figures 3.15 - 3.20. These fields determine the rotational and divergent wind components through the relationships:

$$\overline{V}_r = \overline{k} \times \nabla\psi \qquad (3.1)$$

$$\overline{V}_{div} = \nabla\chi \ . \qquad (3.2)$$

The strength of the wind field is determined by the spacing of isolines in both cases. Though global fields are presented the discussion will center in the tropical latitudes of interest to this

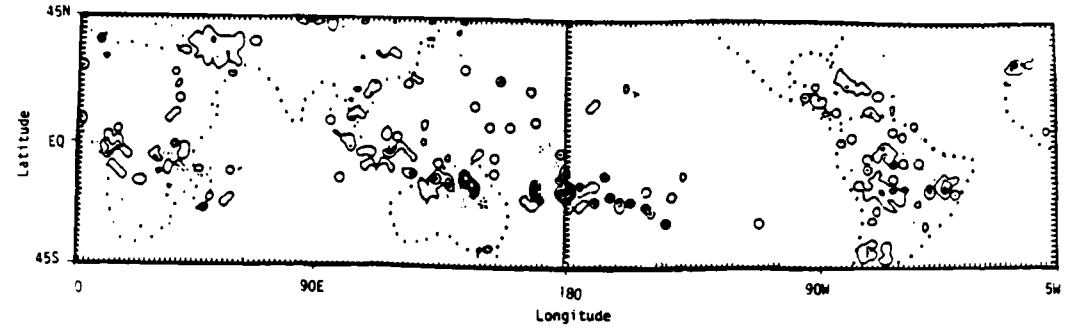

(a)

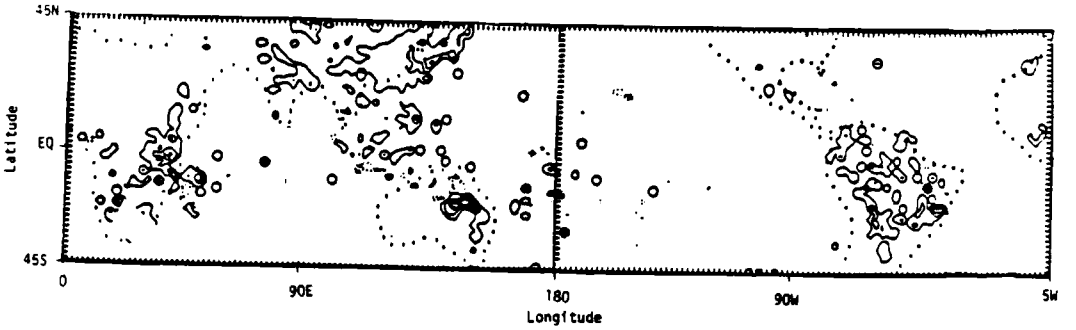

(b)

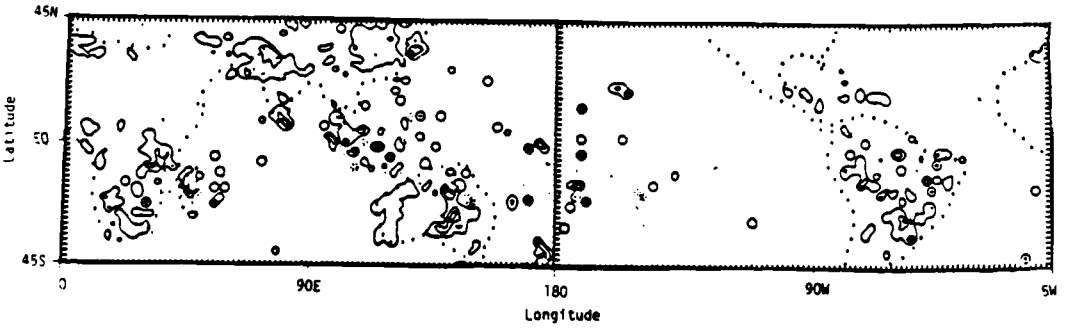

(c)

Figure 3.12. Averaged precipitation amounts differenced from period average (5 January - 1 March, 1979), 1 7/8° x 1 7/8° grid, contour interval of 100.0 x 10^{-1} mm/day. Units are tenths of mm/day, January to February, 1979.

(a) 5 January - 11 January, 1979
(b) 26 January - 1 February, 1979
(c) 16 February - 22 February, 1979

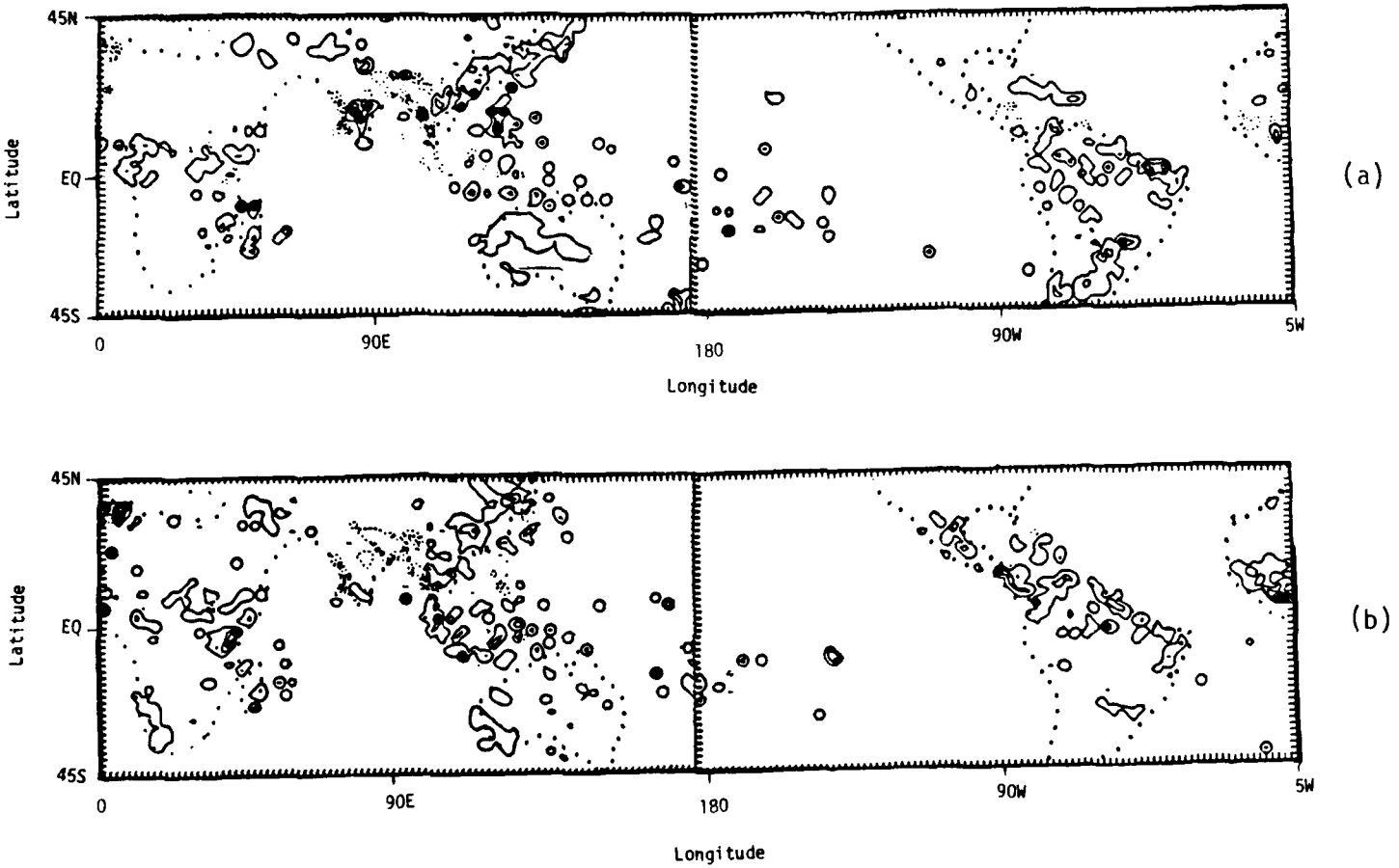

Figure 3.13. Averaged precipitation amounts differenced from period average (5 January - 1 March, 1979), 1 7/8° x 1 7/8° grid, contour interval of 100.00 x 10^{-1} mm/day. Units are tenths of mm/day, May to June, 1979.

(a) 12 May - 18 May, 1979

(b) 2 June - 8 June, 1979

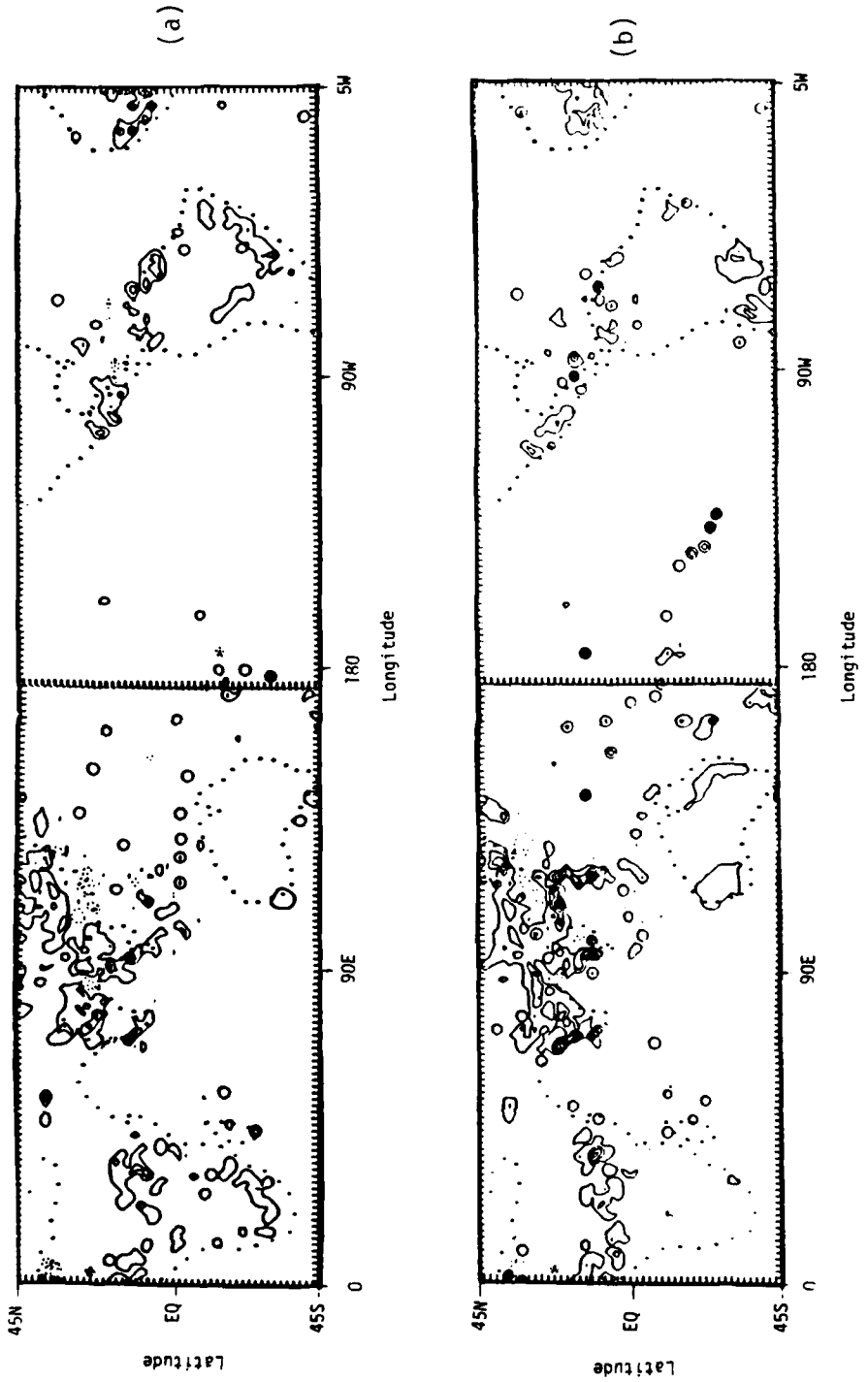

Figure 3.14. Averaged precipitation amounts differenced from period average (5 January - 1 March, 1979), 1 7/8° x 1 7/8° grid, contour interval of 100.0 x 10^{-1} mm/day. Units are tenths of mm/day, July to August, 1979.
(a) 7 July - 13 July, 1979
(b) 28 July - 3 August, 1979

Figure 3.15. Averaged fields, 5 January - 11 January, 1979. Parallel hatched areas represent maximum nondivergent flow strength. Arrows represent direction of divergent or non-divergent flow.

(a) Stream function, 200 mb, contour interval of 25.0 x 10^6 m^2/sec. Units are 10^6 m^2/sec.

(b) Velocity potential, 200 mb, contour interval of 25.0 x 10^5 m^2/sec. Units are 10^5 m^2/sec.

(c) Velocity potential, 850 mb, contour interval of 25.0 x 10^5 m^2/sec. Units are 10^5 m^2/sec.

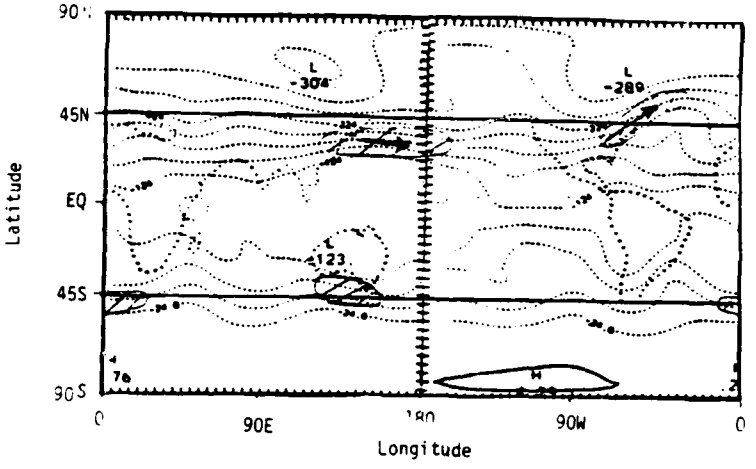
90N
45N
EQ
45S
90S
Latitude
0
90E
180
90W
0
Longitude
L
-304
L
-289
L
-123
H

(a)

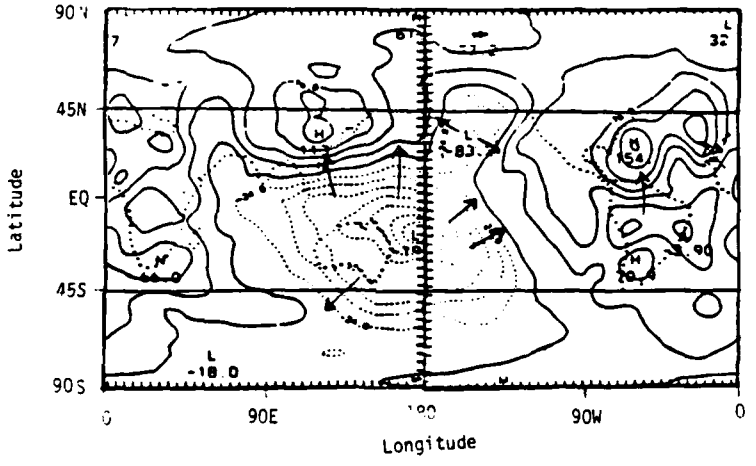
90N
45N
EQ
45S
90S
Latitude
0
90E
180
90W
0
Longitude
L
-83
L
-18.0
H

(b)

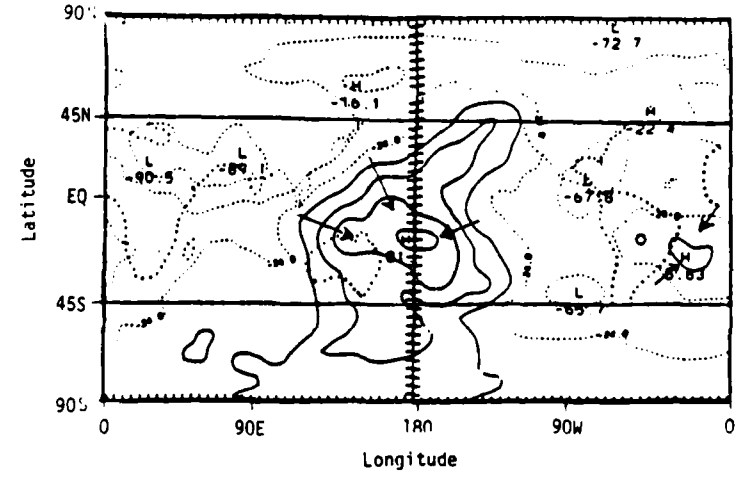
90N
45N
EQ
45S
90S
Latitude
0
90E
180
90W
0
Longitude
L
-72.7
H
-10.1
H
-22.4
L
-90.5
L
-89.1
L
-67.8
L
-65.7

(c)

Figure 3.16. Averaged fields differenced from period average (5 January - 1 March, 1979), 5 January - 11 January, 1979. Parallel hatched areas represent maximum nondivergent flow strength. Arrows represent direction of divergent and nondivergent flow.

(a) Stream function, 200 mb, contour interval of 50.0×10^5 m^2/sec. Units are 10^6 m^2/sec.

(b) Velocity potential, 200 mb, contour interval of 25.0×10^5 m^2/sec. Units are 10^5 m^2/sec.

(c) Stream function, 850 mb, contour interval of 50.0×10^5 m^2/sec. Units are 10^6 m^2/sec.

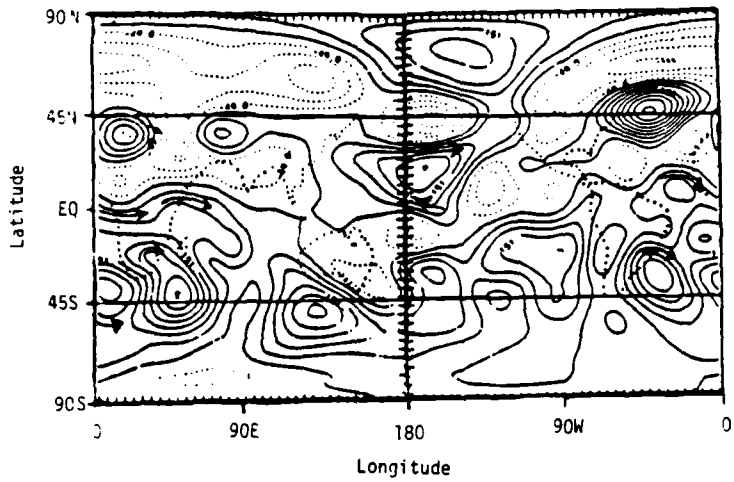
90 N
45 N
EQ
45S
90S
Latitude
0
90E
180
90W
0
Longitude

(a)

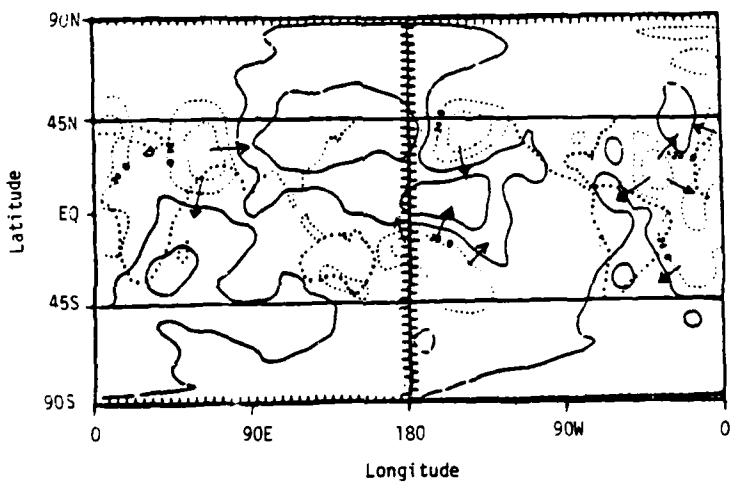
90N
45N
EQ
45S
90S
Latitude
0
90E
180
90W
0
Longitude

(b)

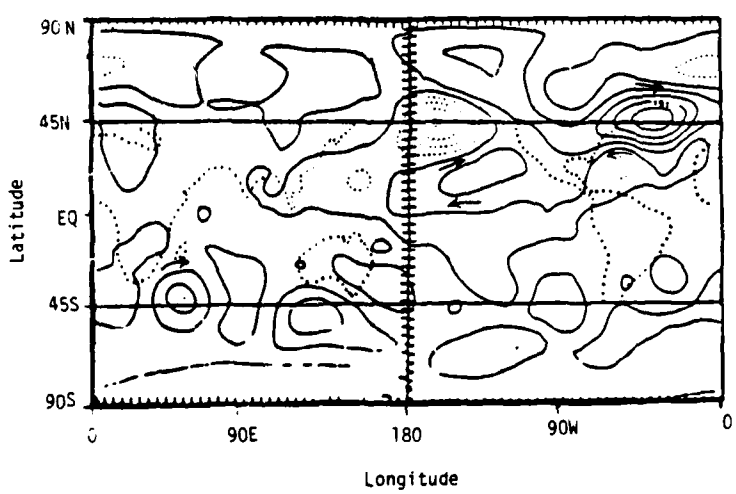
90 N
45N
EQ
45S
90S
Latitude
0
90E
180
90W
0
Longitude

(c)

Figure 3.17. Averaged fields, 26 January - 1 February, 1979. Parallel hatched areas represent maximum non-divergent flow strength. Arrows represent direction of divergent or nondivergent flow.

(a) Stream function, 200 mb, contour interval of 25.0×10^6 m^2/sec. Units are 10^6 m^2/sec.

(b) Velocity potential, 200 mb, contour interval of 25.0×10^5 m^2/sec. Units are 10^5 m^2/sec.

(c) Velocity potential, 850 mb, contour interval of 25.0×10^5 m^2/sec. Units are 10^5 m^2/sec.

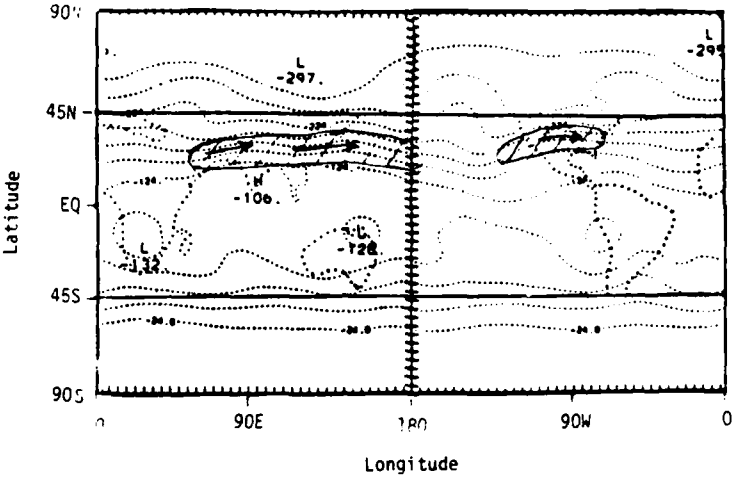
45N
EQ
45S
90S
Latitude
90E
180
90W
0
Longitude

(a)

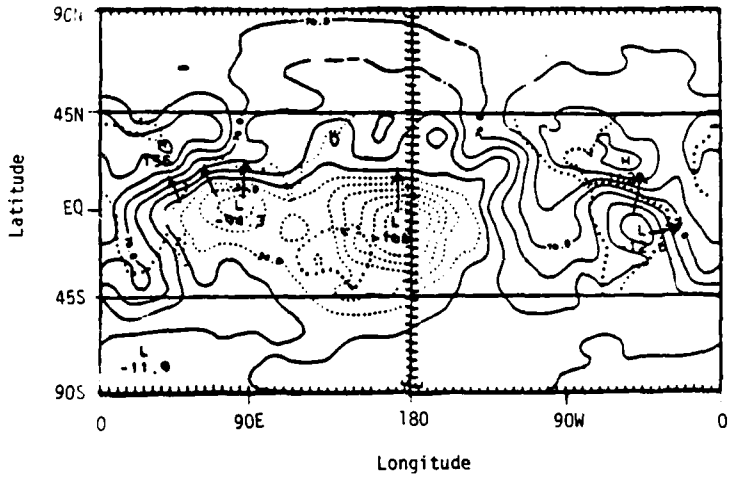
45N
EQ
45S
90S
Latitude
0
90E
180
90W
0
Longitude

(b)

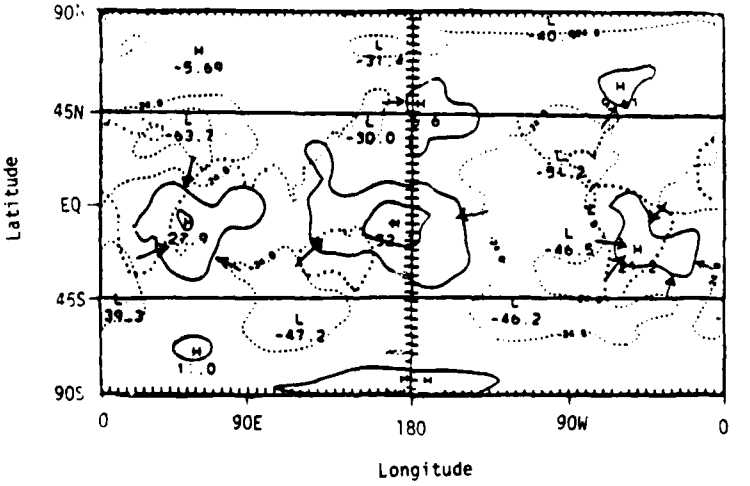
45N
EQ
45S
90S
Latitude
0
90E
180
90W
0
Longitude

(c)

Figure 3.18. Averaged fields differences from period average (5 January - 1 March, 1979), 26 January - 1 February, 1979. Parallel hatched areas represent maximum nondivergent flow strength. Arrows represent direction of divergent and nondivergent flow.

(a) Stream function, 200 mb, contour interval of 50.0 x 10^5 m^2/sec. Units are 10^6 m^2/sec.

(b) Velocity potential, 200 mb, contour interval of 25.0 x 10^5 m^2/sec. Units are 10^5 m^2/sec.

(c) Stream function, 850 mb, contour interval of 50.0 x 10^5 m^2/sec. Units are 10^6 m^2/sec.

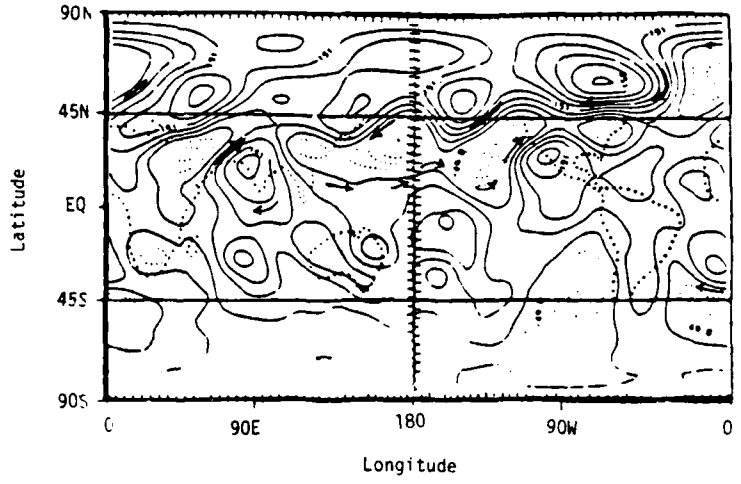
90N
45N
EQ
45S
90S
Latitude
0
90E
180
90W
0
Longitude

(a)

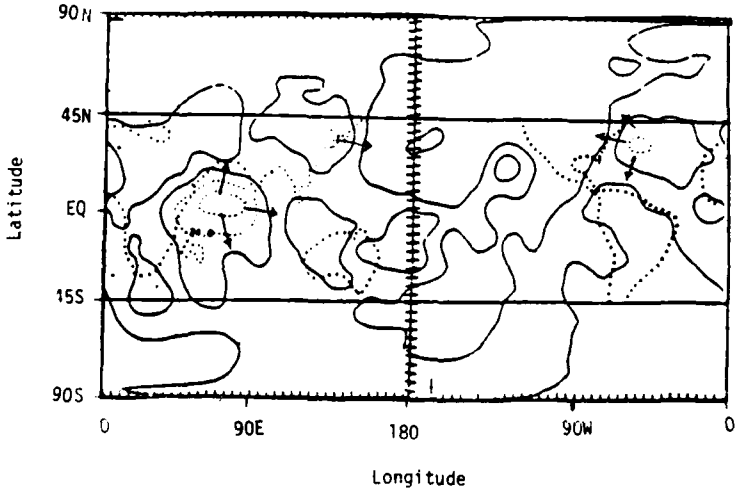
90N
45N
EQ
15S
90S
Latitude
0
90E
180
90W
0
Longitude

(b)

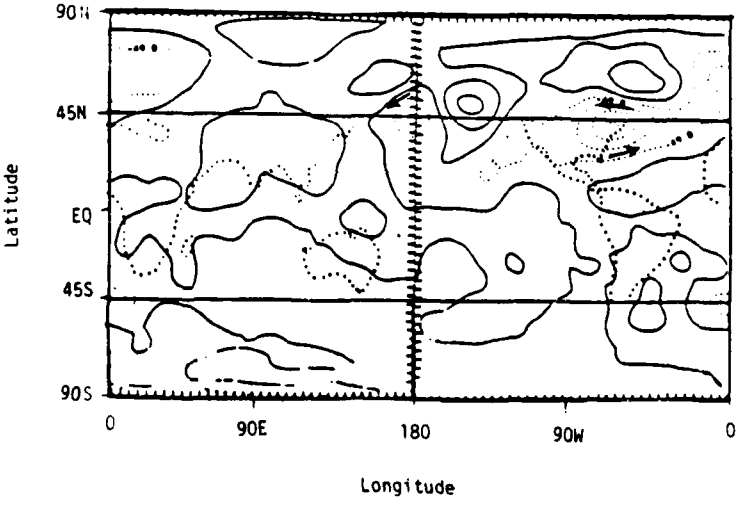
90N
45N
EQ
45S
90S
Latitude
0
90E
180
90W
0
Longitude

(c)

Figure 3.19. Averaged fields, 16 February - 22 February, 1979. Parallel hatched areas represent maximum nondivergent flow strength. Arrows represent direction of divergent or non-divergent flow.

(a) Stream function, 200 mb, contour interval of 25.0×10^6 m^2/sec. Units are 10^6 m^2/sec.

(b) Velocity potential, 200 mb, contour interval of 25.0×10^5 m^2/sec. Units are 10^5 m^2/sec.

(c) Velocity potential, 850 mb, contour interval of 25.0×10^5 m^2/sec. Units are 10^5 m^2/sec.

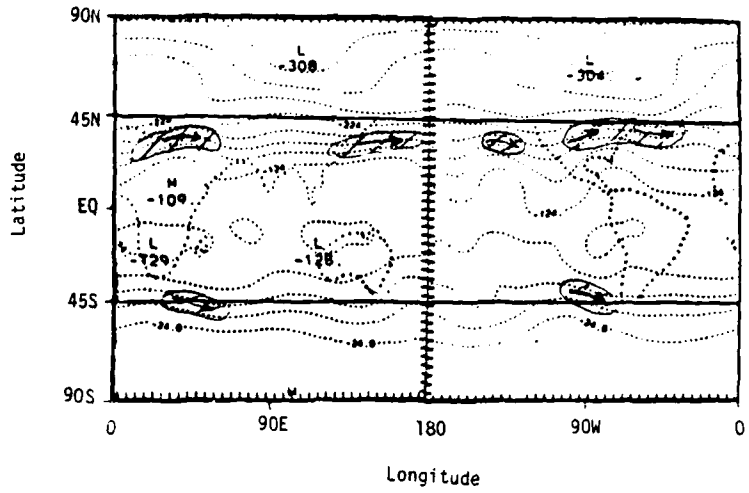
90N
45N
EQ
45S
90S
Latitude
0
90E
180
90W
0
Longitude

(a)

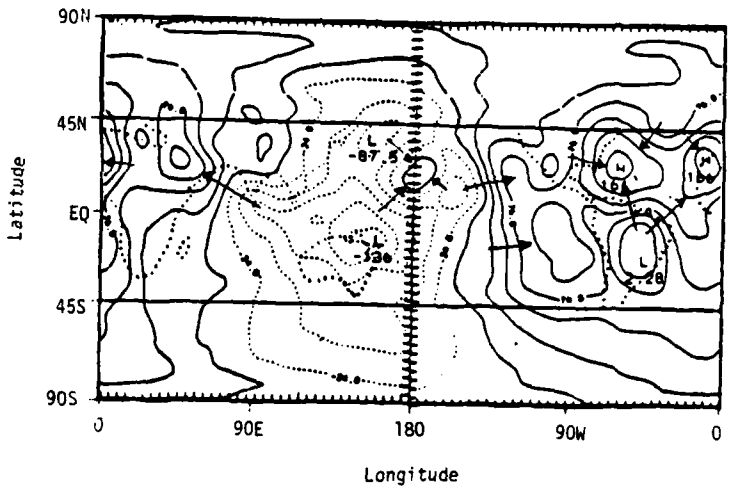
90N
45N
EQ
45S
90S
Latitude
0
90E
180
90W
0
Longitude

(b)

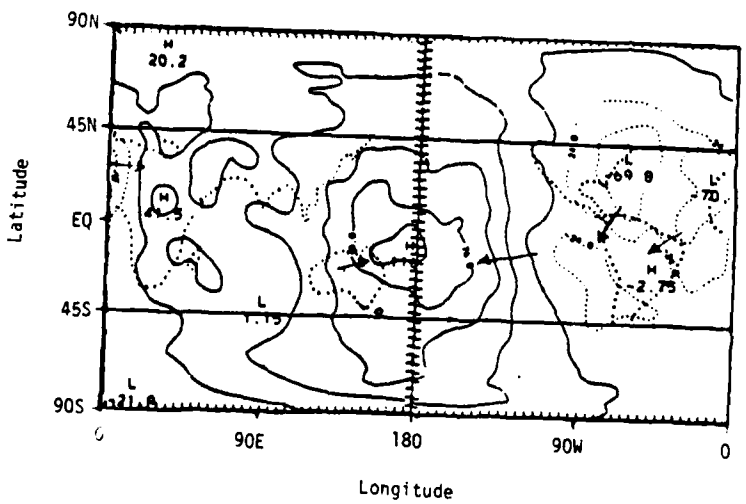
90N
45N
EQ
45S
90S
Latitude
0
90E
180
90W
0
Longitude

(c)

Figure 3.20. Averaged fields differenced from period average (5 January - 1 March, 1979), 16 February - 22 February, 1979. Parallel hatched areas represent maximum nondivergent flow strength. Arrows represent direction of divergent and nondivergent flow.

(a) Stream function, 200 mb, contour interval of 50.0×10^5 m^2/sec. Units are 10^6 m^2/sec.

(b) Velocity potential, 200 mb, contour interval of 25.0×10^5 m^2/sec. Units are 10^5 m^2/sec.

(c) Stream function, 850 mb, contour interval of 50.0×10^5 m^2/sec. Units are 10^6 m^2/sec.

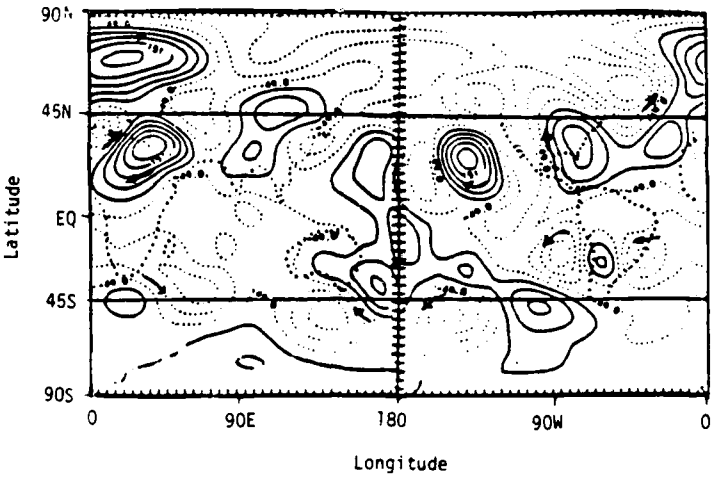
90N
45N
EQ
45S
90S
Latitude
0
90E
180
90W
0
Longitude

(a)

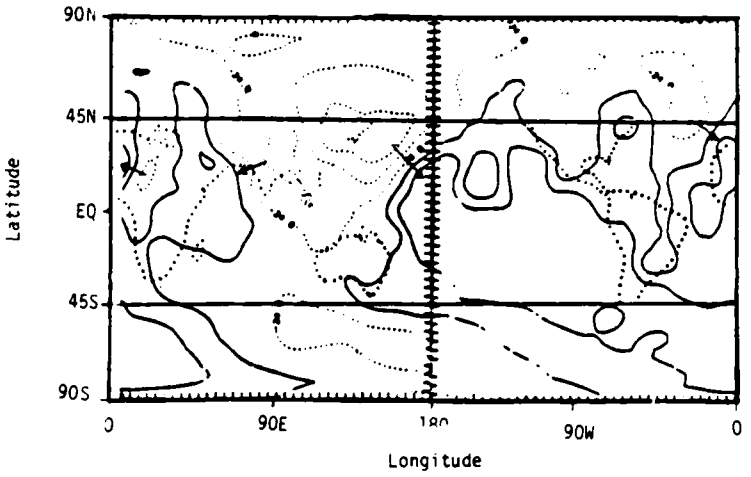
90N
45N
EQ
45S
90S
Latitude
0
90E
180
90W
0
Longitude

(b)

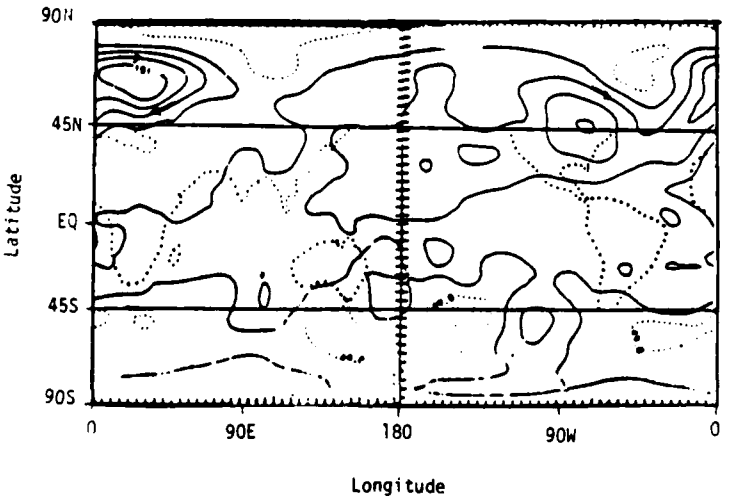
90N
45N
EQ
45S
90S
Latitude
0
90E
180
90W
0
Longitude

(c)

study. Divergence aloft and convergence in lower levels correspond to higher tropical precipitation and heating values. At extra-tropical latitudes the contribution from latent heat release to the total heating field is small.

The week of January 5 - 11 is characterized by strong divergent motions emanating from the central Pacific and South Pacific Convergence Zone where precipitation and heating maxima are located. Another divergence center is located over South America. Strong subtropical westerly jets in the Northern Hemisophere are found at similar longitudes. Sampson (1982) documented similar relationships in his weekly analysis of FGGE data. The 200 mb anomalies (defined as differences from seasonal averages) indicate that these two divergence centers are stronger than the seasonal averages and are found in general in conjunction with equatorial westerlies. The week of January 26 - February 1 displays divergent circulation over South America and the dateline close to seasonal values. The main divergent flow anomaly is centered over the Indian Ocean in apparent response to the heating anomaly previously discussed. Equatorial easterlies are found in the 200 mb anomaly chart over and to the west of the velocity potential minimum with westerlies to the east. The week of February 16 - 22 is similar to the seasonal averages over the Southern Hemisphere tropics, while a divergence anomaly is apparent over Nigeria.

These pulsations of tropical convection and related overturnings may be partly due to a long periodicity perturbation (such as the 30 - 50 day wave) propagating through the global tropics.

3.4 Daily Variations

Rainfall rates are compared with heating rates, integrated over a column from about 250 to 600 mb every 6 hours. Heat changes are plotted for every tenth degree centigrade and rainfall rates are plotted for every millimeter/day. The selected mid atmospheric heating rates are chosen to better represent latent heat release. Five different areas are plotted. The five areas investigate portions of South America (Figure 3.21), the Indian Ocean (Figure 3.21), the South Pacific (Figure 3.21), Australia (Figure 3.22), and Africa (Figure 3.22). Area boundaries are: South America - 4 degrees south, 21 degrees south. 43 degrees west, 58 degrees west; the Indian Ocean - 4 degrees north, 11 degrees south, 49 degrees east, 79 degrees east; the South Pacific - 11 degrees south, 24 degrees south, 142 degrees west, 167 degrees west; Australia - 4 degrees south, 17 degrees south, 131 degrees east, 152 degrees east; and Africa - 4 degrees south, 21 degrees south, 23 degrees east, 43 degrees east. They are plotted over a 55 day period.

Variability increases in one field are related to greater variability in the other field. Both variables appear to increase and decrease in a similar fashion. The largest precipitation rates are found over the SPCZ during the first 2 weeks of SOP-1. This area shows higher heating rates when there are higher precipitation rates. Other areas do not exhibit the dramatic long term change from high to low rates within the 55 day period, as does the South Pacific area, though other oscillations with time scales of 1 to 2 weeks can be detected in these graphs. The heating rates have a strong semi-diurnal component.

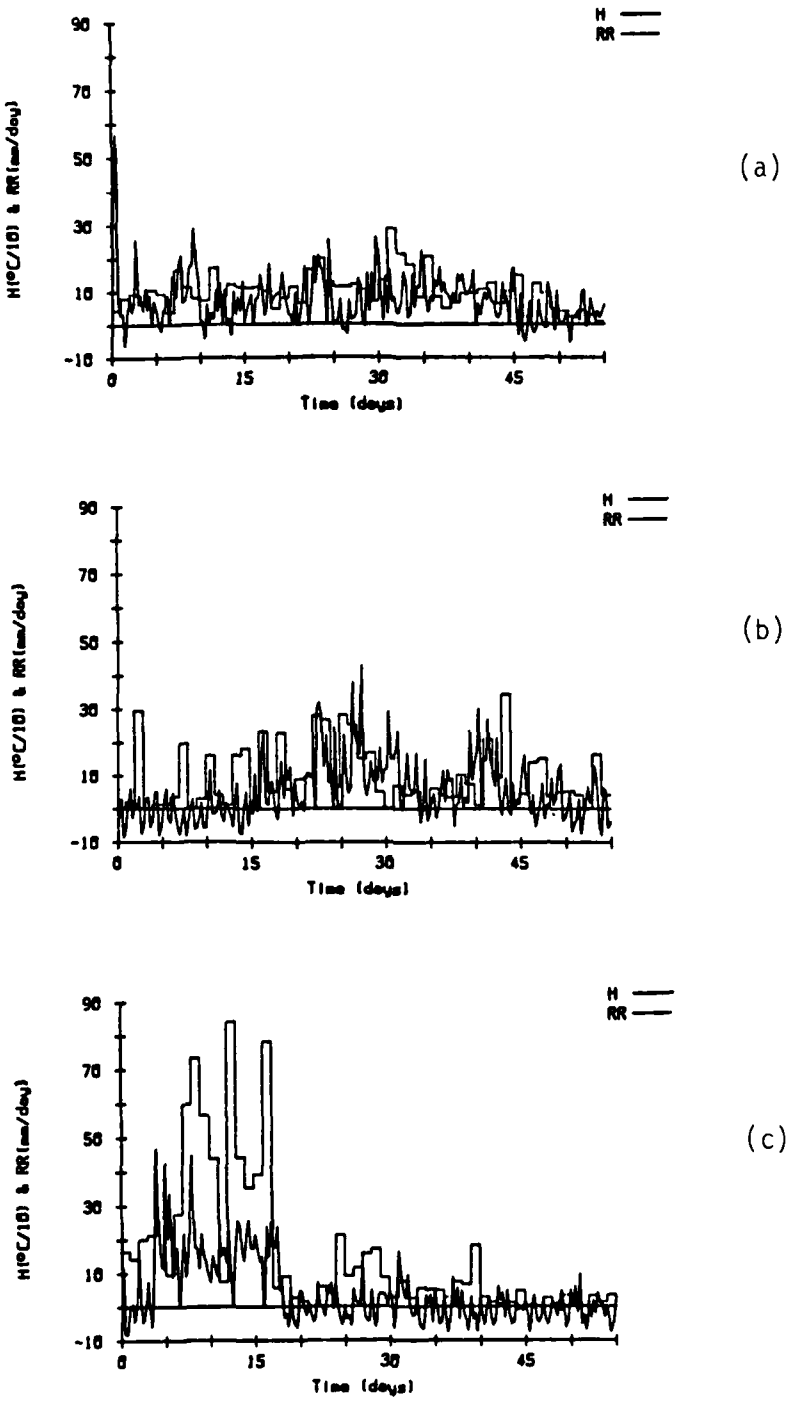

Figure 3.21. Heating and rainfall rates versus time, 5 January - 28 February, 1979, South America, Indian Ocean, and South Pacific.
(a) South America, 12 to 29 reporting stations per day
(b) Indian Ocean, 0 to 4 reporting stations per day
(c) South Pacific, 7 to 8 reporting stations per day

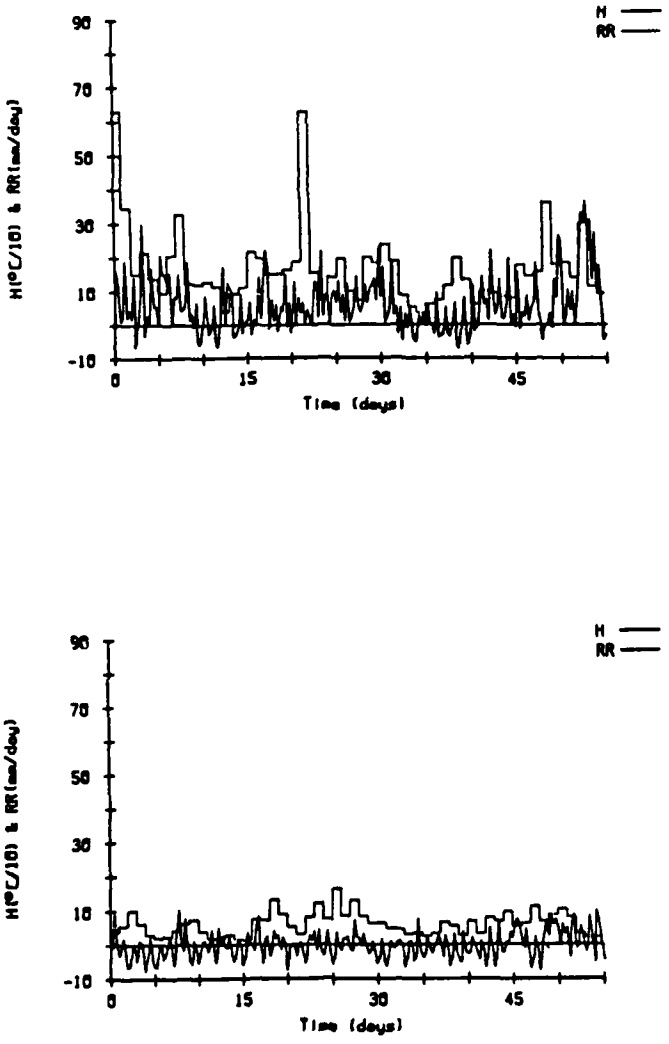

Figure 3.22. Heating and rainfall rates versus time, 5 January - 28 February, 1979, Australia and Africa.
(a) Australia, 257 to 300 reporting stations per day
(b) Africa, 40 to 67 reporting stations per day

3.5 Hourly Averages

The differences between the circulation models and the differences from 00 GMT are displayed. The GLAS heating rates at 00 GMT and the differences from 00 GMT are shown on Figure 3.23 and velocity potentials from ECMWF, GFDL, and GLAS/NASA analysis models are displayed in Figures 3.24 - 3.26.

The high heating rates over South America do not have the intense divergence at 200 mb as other high heating rate areas produced by these models. All the models match areas of upper level divergence with higher heating rates, and areas of upper level convergence with lower heating rates.

The heat field differences from 00 GMT show an apparent movement with time. The positive heating rates follow the daylight hours. Land masses probably influence this diurnal trend by distorting heating rates toward positive values over longitudes corresponding to these areas. The flux of incoming and outgoing radiation seems to assert a greater effect on the heating rates. This effect could also be due to extended areas of increased daytime cumulus convective activity, especially over land masses, but should be more localized than seen on the charts. Since the GLAS heating rate differences and GLAS velocity potential differences are from the same model they show a relationship; whereas the other two models do not. This relationship indicates the consistency between the first guess of the model and the actual data. The flow intensity changes of the divergence field aligns mostly along and inside the border of the positive heating area (Figures 3.23, 3.24, and 3.26). Most areas decrease the original divergent flow in response to the boundaries of

Figure 3.23. Averaged column integrated heating rates, 5 January - 11 January, 1979, contour interval of 50.0 x 10^{-1}°C/day. Units are tenths of degrees Centigrade/day.

(a) 00Z
(b) 06Z differenced from 00Z
(c) 12Z differenced from 00Z
(d) 18Z differenced from 00Z

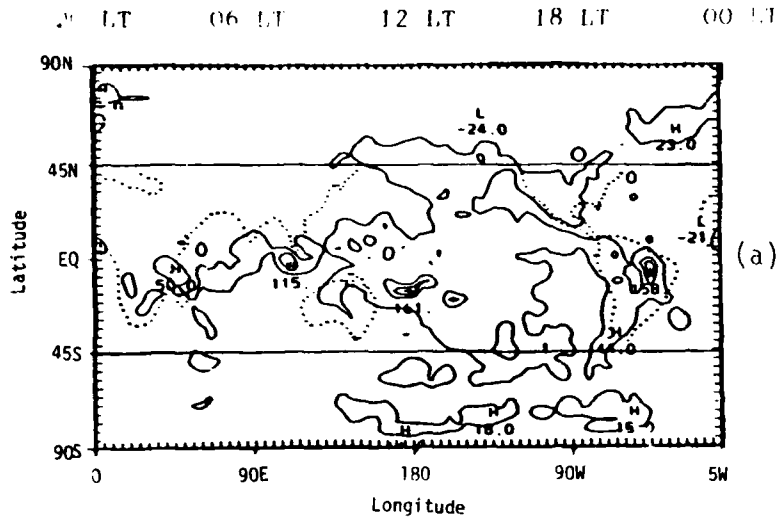
LT 06 LT 12 LT 18 LT 00 LT
90N
45N
EQ
45S
90S
Latitude
0
90E
180
90W
5W
Longitude
(a)

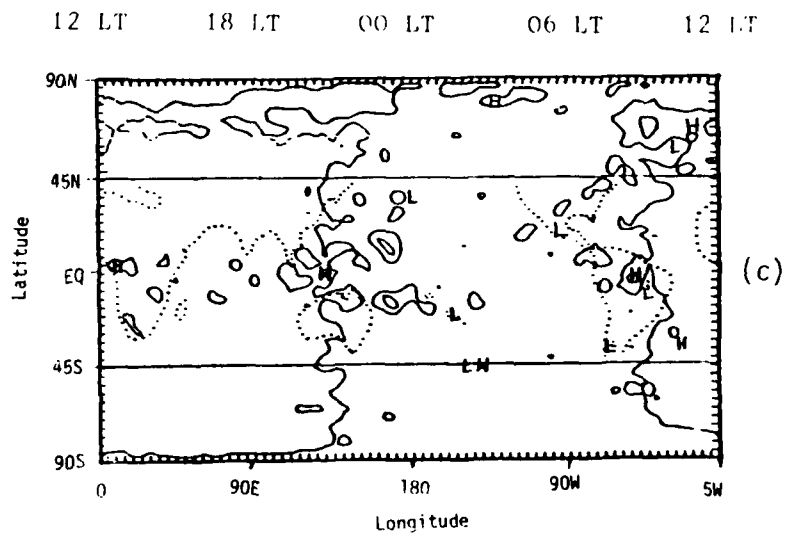
12 LT 18 LT 00 LT 06 LT 12 LT
90N
45N
EQ
45S
90S
Latitude
0
90E
180
90W
5W
Longitude
(c)

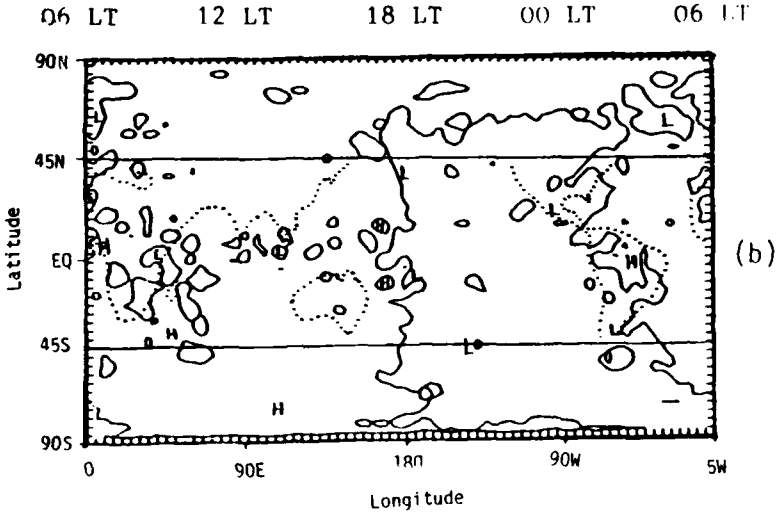
06 LT 12 LT 18 LT 00 LT 06 LT
90N
45N
EQ
45S
90S
Latitude
0
90E
180
90W
5W
Longitude
(b)

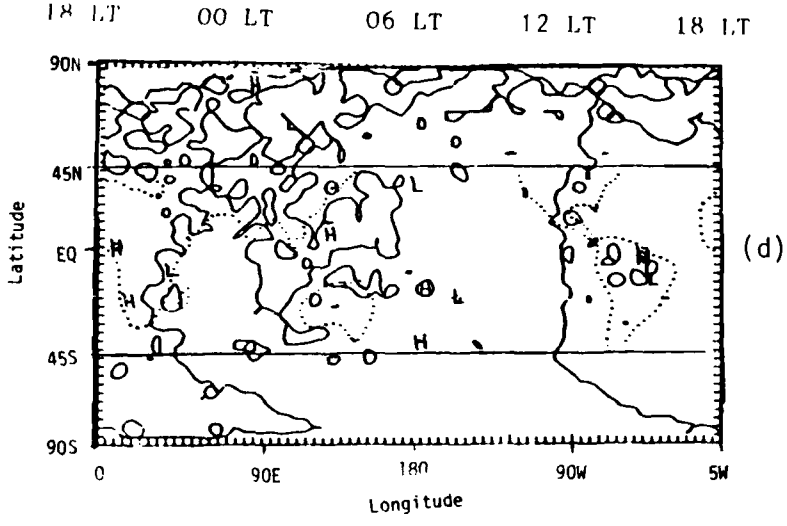
18 LT 00 LT 06 LT 12 LT 18 LT
90N
45N
EQ
45S
90S
Latitude
0
90E
180
90W
5W
Longitude
(d)

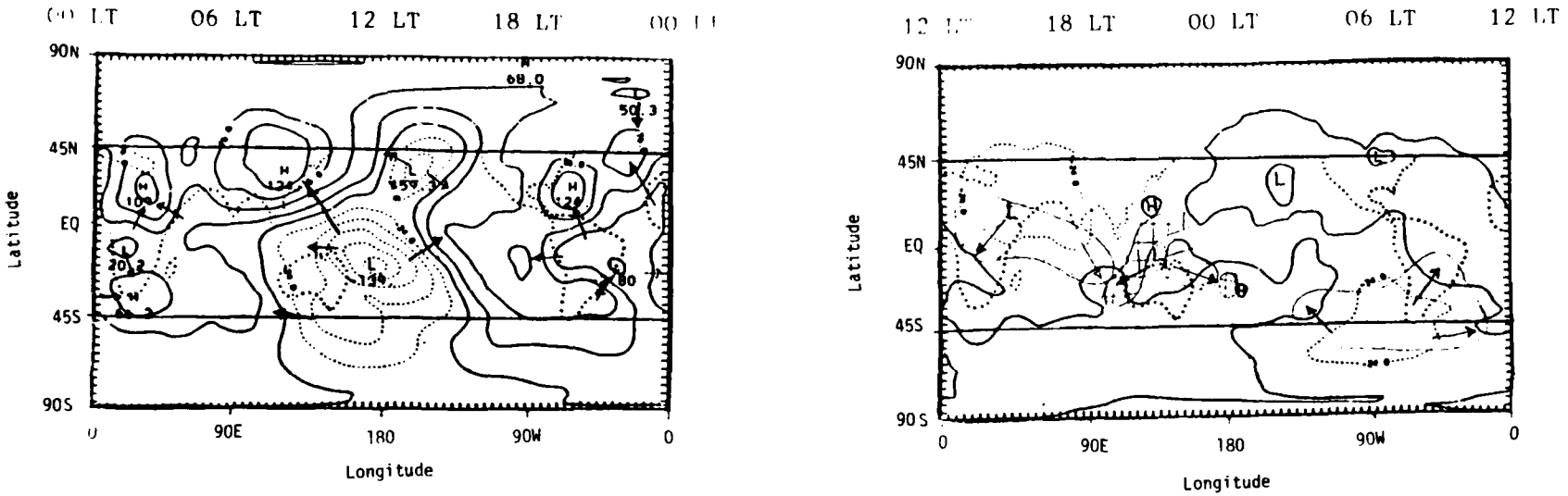

(a) (b)

Figure 3.24. Averaged velocity potential fields, 5 January - 11 January, 1979, ECMWF data set, 200 mb, contour interval of 25.0 x 10^5 m^2/sec. Units are 10^5 m^2/sec. Cross hatched areas represent increase divergent flow from 00Z. Parallel hatched areas represent decrease divergent flow from 00Z. Arrows represent direction of divergent flow.

(a) 00Z
(b) 12Z differenced from 00Z

Figure 3.25. Averaged velocity potential fields, 5 January - 11 January, 1979, GFDL data set, 200 mb, contour interval of 25.0 x 10^5 m^2/sec. Units are 10^5 m^2/sec. Cross hatched areas represent increase divergent flow from 00Z. Parallel hatched areas represent decrease divergent flow from 00Z. Arrows represent direction of divergent flow.

(a) 00Z
(b) 06Z differenced from 00Z
(c) 12Z differenced from 00Z
(d) 18Z differenced from 00Z

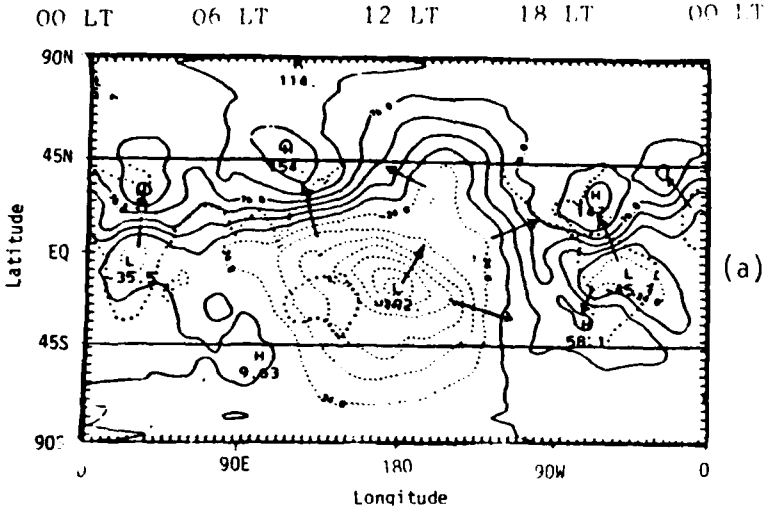
00 LT
06 LT
12 LT
18 LT
00 LT
90N
45N
EQ
45S
90S
Latitude
0
90E
180
90W
0
Longitude
(a)

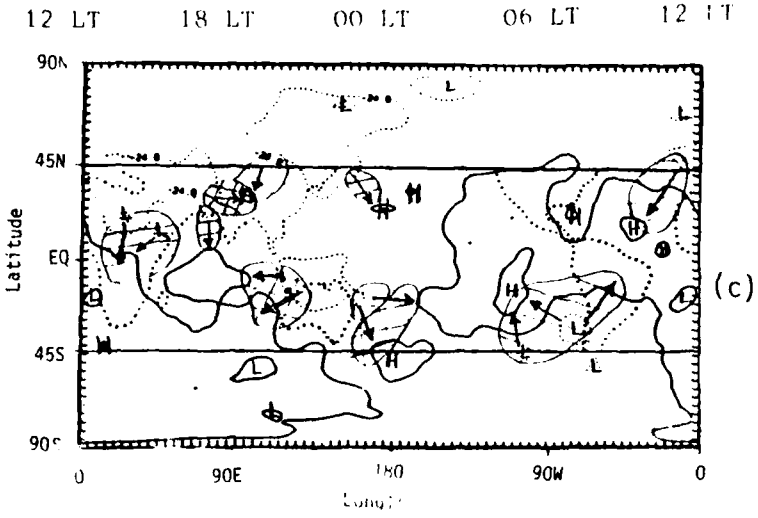
12 LT
18 LT
00 LT
06 LT
12 LT
90N
45N
EQ
45S
90S
Latitude
0
90E
180
90W
0
(c)

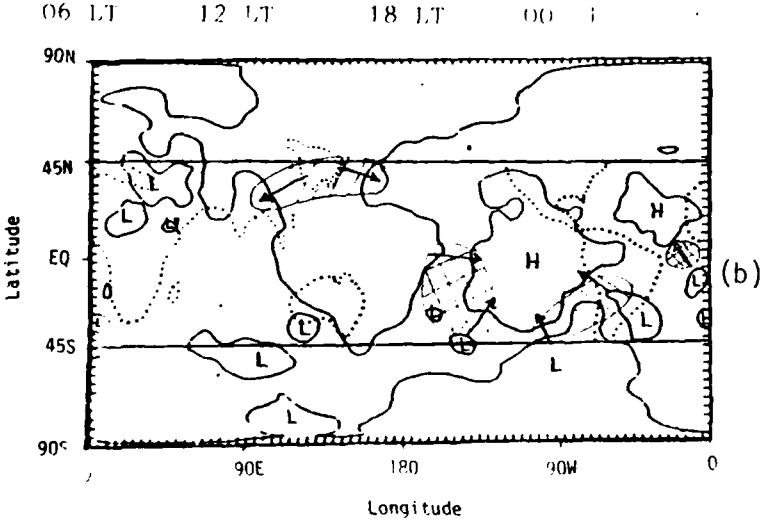
06 LT
12 LT
18 LT
90N
45N
EQ
45S
90S
Latitude
0
90E
180
90W
0
Longitude
(b)

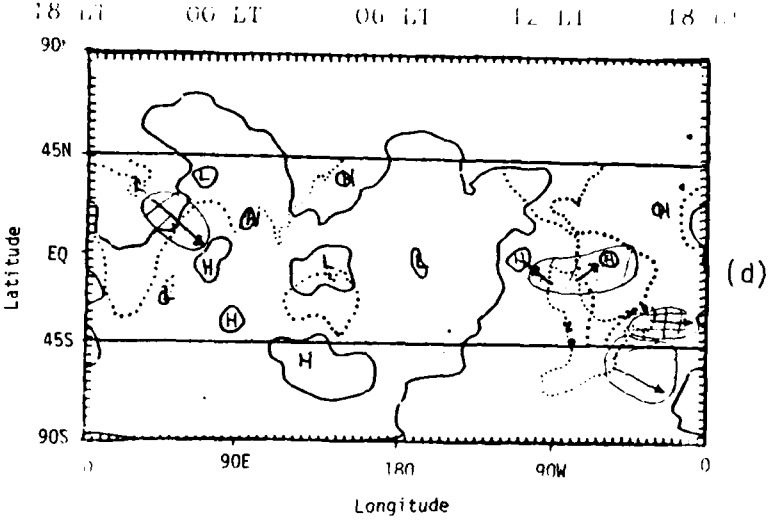
06 LT
06 LT
45N
EQ
45S
90S
Latitude
0
90E
180
90W
0
Longitude
(d)

Figure 3.26. Averaged velocity potential fields, 5 January - 11 January, 1979, GLAS data set, 200 mb, contour interval of 25.0 x 10^5 m^2/sec. Units are 10^5 m^2/sec. Cross hatched areas represent increase divergent flow from 00Z. Parallel hatched ares represent decrease divergent flow from 00Z. Arrows represent direction of divergent flow.

(a) 06Z differenced from 00Z
(b) 12Z differenced from 00Z
(c) 18Z differenced from 00Z

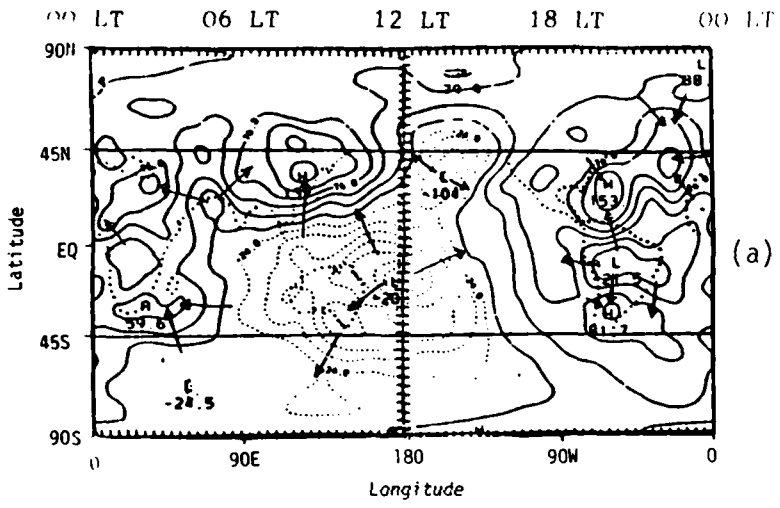
00 LT
06 LT
12 LT
18 LT
00 LT
90N
45N
EQ
45S
90S
Latitude
0
90E
180
90W
0
Longitude
(a)

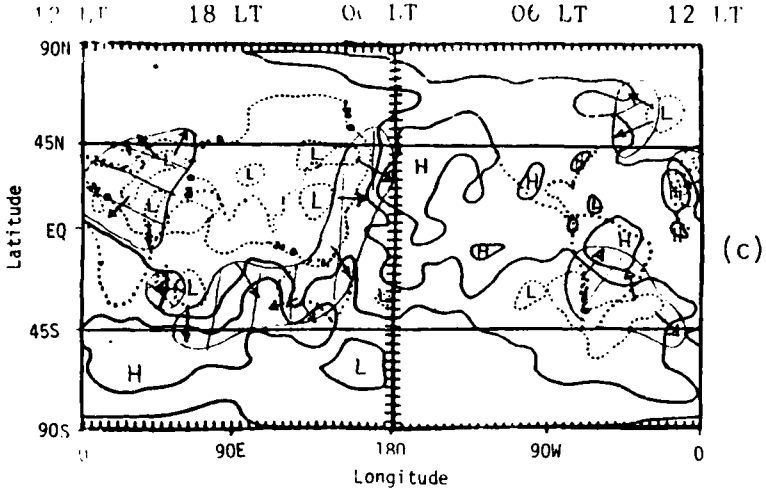
18 LT
06 LT
06 LT
12 LT
90N
45N
EQ
45S
90S
Latitude
90E
180
90W
0
Longitude
(c)

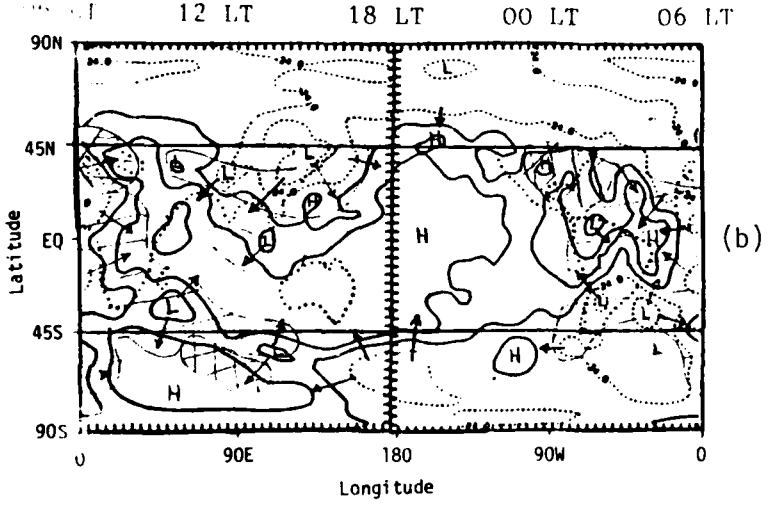
12 LT
18 LT
00 LT
06 LT
90N
45N
EQ
45S
90S
Latitude
0
90E
180
90W
0
Longitude
(b)

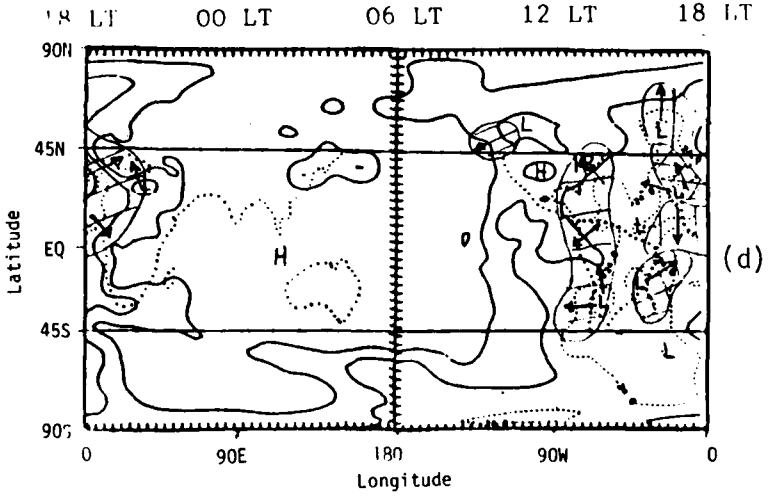
18 LT
00 LT
06 LT
12 LT
18 LT
90N
45N
EQ
45S
90S
Latitude
0
90E
180
90W
0
Longitude
(d)

cooling and heating. It must be remembered there is a correspondence between the precipitation fields, the velocity potentials (divergence), and heating rates, since latent heat release is a component of the heating rates.

The individual velocity potential patterns at 00 GMT (Figures 3.24 - 3.26) of the three models are very similar, but when intensities are viewed, one model is much different than the others. The GLAS and GFDL data look quite similar, but the ECMWF values are much smaller. The center values in the GLAS and GFDL models are quite close to each other. The GLAS and the ECMWF fields agree where the two lobes of the velocity potential come off the deepest low center; the GFDL field does not. The GLAS and ECMWF fields emphasize the northern lobe and GFDL fields emphasize the western lobe. These results agree with results mentioned in the circulation acquisition section. That is, the GFDL model has stronger divergent flow and shallower troughs compared to the ECMWF model.

The differences from 00 GMT (Figures 3.24 - 3.26) show GLAS values having a much greater change form the 00 GMT data than the other two fields. The ECMWF data have the smoothest appearance. The change of the divergent flow with time is another apsect of these differences. The GLAS model has much greater flow intensity changes of velocity potential than the other two models (Figures 3.24 - 3.26), with intensity changes occurring in different areas. Also, the continents can influence the difference fields. Good examples are the GLAS differenced fields (Figure 3.26) over South America at 06 GMT, Africa at 12 GMT, and the east coast of North America at 18 GMT. The other models show the same relationship having most

areas either over continents or divided by their coastlines. Also, there is a diurnal trend towards a decrease or increase of divergent flow favoring oncontinental 200 mb flow late evening to early morning and offcontinental 200 mb flow during the afternoon and early evening, for example, over Asia and South America. Between those times the changes in divergent flow and area of change decrease.

Here, again, all three fields have similar appearances. Overall, the GLAS field has greater change with time, the ECMWF data have much lower intensities, and the GFDL field has shallower troughs.

CHAPTER 4

CONCLUSIONS

4.1 Data

The purpose of this study is to take the FGGE precipitation data and to put it into a usable form. This is accomplished by using data that are without error, averaging that data over time and space, and arranging the grids of data on a world format. This is done from 45° north to 45° south for daily averages over various periods (seasonal, weekly, and daily).

The data are compared to climatology and other fields created from the FGGE data. Although it has been noted that the GWE year was atypical (Paegle, 1984), the results here show a general trend of correspondence between the data. Of course, there are regions of disagreement and uncertainty. Some of the uncertainty can come from the precipitation data being quite different from precipitation values a short distance away but, overall, the values are fairly representative, especially over areas of dense observations. Another direct problem is the scarcity of, or nonexistence of, data in certain locations, especially over the oceans.

The seasonal charts show northward movement of rainfall maxima from winter to summer, with higher than normal values located over Morocco, Cape York (Australia), and Madagascar. Higher heating rates correspond to higher rainfall rates, although heating rates are low

over Madagascar, SPCZ, northwest Africa, and northeast Australia, and high over the Amazon basin. The U and V wind components have no western maxima over the Arabian penninsula and South America, have a stronger jet east of Australia and south of Africa, both 15 degrees further south, and have stronger meridional motions associated with convective tropical regions, when compared to extended climatology.

The weekly charts have an overall trend of high rainfall rates over high heating rates, with the same correspondence as the seasons. Values of up to 8 cm/day are recorded over India and the northeast coast of Australia. Also identified is a 3 week oscillation between high rainfall rates over the Indian Ocean and dateline. The divergence aloft corresponds with higher heating rates and rainfall rates, and oscillates, as above.

The daily variations for selected areas show heating rates having semidiurnal fluctuations. As the variability of the heating rates increase, the rainfall rates increase. These variables appear to increase and decrease together.

The hourly heating rates, rainfall rates, and convergence again correspond as above relations. There is an apparent movement of positive heating values with daylight hours, although distorted over land masses. Divergent flow changes occur mainly along and inside the positive value area in the GLAS model. The increase or decrease of the velocity potential flow also changes diurnally. The daylight hours favor offcontinental 200 mb flow; whereas the late evening to early morning hours favor oncontinental 200 mb flow. This also is an apparent influence of the velocity potential differences by the continents. The ECMWF model has lower divergence intensities, the GLAS

model has greater change with time, and the GFDL model has shallower troughs.

Some of the regional differences are also probably attributable to the following factors: land cover (which affects the amount of radiation retained), latitude (which determines which heat component is dominant), amount of nonprecipitating clouds, observational density, sea surface temperatures, and many others. These regional differences need to be studied in more depth in the future.

4.2 Future Studies

More can be done to this material to make it more complete. The use of satellite data is easily accessible. The TIROS Operational Vertical Sounder (TOVS) system can be used to get global coverage (e.g., Susskind, et al., 1984). A recent development in using the microwave measurement of water vapor is yielding very good results over the oceans. It can measure precipitable water versus nonprecipitating clouds. For these results the NIMBUS 7 Scanning Multichannel Microwave Radiometer (SMMR) data derived by Hwang, et al. (1984) could be used for precipitation data over the oceans if future research developments provide surface rainfall rates. Due to the sparseness of the data over the oceans, the increase of this information would greatly add to the data input from these areas on future studies. The data were also gathered for the period from December 1978 through November 1979, the same time frame as the FGGE period.

REFERENCES

Baker, W. E., 1983: Objective Analysis and Assimilation of Observational Data from FGGE. Mon. Wea. Rev., 111, 328-242.

Baker, W. E., and J. Paegle, 1983: The Influence of Tropics on the Prediction of Ultralong Waves. Part I: Tropical Wind Field. Mon. Wea. Rev., 111, 1341-1355.

Bengtsson, Lennart, 1983: The ECMWF Level III-B Data Set. U.S. Committee for GARP, GWE Newsletter, 1, 1-7.

Carr, Frederick H., and Mohan Ramamurthy, 1983: Comparison of II-a and III-b Analyses during the Monsoon Onset Period. U.S. Committee for GARP, GWE Newsletter, 1, 27-28.

Holton, James R., 1979: An Introduction to Dynamic Meteorology. Academic Press, New York, 323-324, 328-329.

Hwang, P. H., T. T. Wilheit, and A. T. C. Chang, 1984: Monthly Distributions of Precipitable Water from the NUMBUS 7 SMMR Data. J. Geophy. Research, 89, 5328-5334.

Johnson, D. R., 1980: A Generalized Transport Equation for Use with Meteorological Coordinate Systems. Mon. Wea. Rev., 108, 733-745.

Julian, Paul R., 1983: Comments on the ECMWF IIIb Analysis Data Set. U.S. Committee for GARP, GWE Newsletter, 1, 15-17.

Kalnay, E., and W. E. Baker, 1984: Analyzed and Diagnosed Fields in the GLAS FGGE III-b Analysis. U.S. Committee for GARP, GWE Newsletter, 3, 29-31.

Karoly, David J., A. Graeme, M. Kelly, and J. F. Le Marshall, 1983: Interannual Variability of the Southern Hemisphere Troposphere. Preprint Vol. of Extended Abstracts: First Inter. Conf. on S. Hemi. Meteo. July 31 - Aug. 6, 1983. Sao Jose Dos Campos, Brazil. American Meteorological Society, Boston, Mass., 44-46.

Kasahara, Akira, and Arthur Mizzi, 1983: Diurnal Variations of the Divergence Field in the ECMWF Level III-B Analysis Data. U.S. Committee for GARP, GWE Newsletter, 2, 5-11.

Kasahara, Akira, and Arthur P. Mizzi, 1983: On the Evaluation of the Heating/Cooling Rate from the ECMWF Level III-b Analysis Data. U.S. Committee for GARP, GWE Newsletter, 2, 12-17.

Krishnamurti, T. N., and S. Gadgil, 1984: On the Structure of the 30 to 50 Day Mode over the Globe during FGGE. Florida State University Report No: 84-1, 1-26.

Krishnamurti, T. N., P. K. Jayakumar, Jian Sheng, Naomi Surgi, and Arun Kumar, 1984: Divergent Circulations on the 30 to 50 Day Time Scale. (Submitted for publication to the J. Atmos. Sci.).

Krishnamurti, T. N., and D. Subrahmanyan, 1982: The 30 - 50 Day Mode at 850 mb during MONEX. J. Atmos. Sci., 39, 2088-2095.

Lambert, Steven J., 1983: List of Known or Suspected Problems with the ECMWF Analyses of FGGE Data. U.S. Committee for GARP, GWE Newsletter, 1, 25-26.

Lorenc, C., 1984: The Evolution of Planetary Scale 200 mb Divergence during the FGGE Year. Meteorological Office Technical Note No. II/210, 1-23. Available from Dynamical Climatology Branch, Meteorological Office, London Road, Bracknell, Berkshire, England.

Luo, H., and M. Yanai, 1984: The General Circulation and Heat Sources over the Tibetan Plateau and Surrounding Areas during the Onset of the 1979 Monsoon. Inter. Symposium on the Qinghai-Xizang (Tibet) Plateau on Mountain Meteor. Beijing, People's Republic of China. March, 1984 (in press).

Madden, R. A., and P. R. Julian, 1971: Detection of a 40 - 50 Day Oscillation in the Zonal Wind in the Tropical Pacific. J. Atmos. Sci., 28, 702-708.

Madden, R. A., and P. R. Julian, 1972: Description of Global-Scale Circulation Cells in the Tropics with a 40 - 50 Day Period. J. Atmos. Sci., 29, 1109-1123.

Miyakado, K., J. Ploshay, and W. Stern, 1983: Guide and Caution on the the GFDL/FGGE III-B Data Set. U.S. Committee for GARP, GWE Newsletter, 1, 8-14.

Murakami, T., and Y. H. Ding, 1982: Wind and Temperature Changes on Eurasia during the Early Summer of 1979. J. Meteor. Soc. Japan, 60, 183-196.

Newell, Reginald E., John W. Kidson, Dayton G. Vincent, and George J. Boer, 1973: The General Circulation of the Tropical Atmosphere and Interactions with Extratropical Latitudes. Massachusetts Institute of Technology Press, Cambridge, Massachusetts and London, England, 1 and 2, 98, 116, 164-165.

Paegle, Jan, and Wayman E. Baker, 1983: The Influence of the Tropics on the Prediction of Ultralong Waves. Part II: Latent Heating. Mon. Wea. Rev., 111, 1356-1371.

Paegle, Jan, and Julia N. Paegle, 1984: GLAS Heating Rate Estimates for SOP-1. U.S. Committee for GARP, GWE Newsletter, 3, 25-28.

Paegle, Jan, and Edward Mason Tomlinson, 1975: Solution of the Balance Equation by Fourier Transform and Gauss Elimination. Mon. Wea. Rev., 103, 528-535.

Paegle, Julia N., 1983: Some Characteristics of ECMWF Level III-b Data Sets. U.S. Committee for GARP, GWE Newsletter, 1, 18-22.

Paegle, Julia N., 1984: First International Conference on Southern Hemisphere Meteorology, 31 July - 6 August, 1983, Sao Jose dos Campos, Brazil. Bul. Amer. Meteor. Soc., 65, 48-54.

Paegle, Julia N., Fred P. Lewis, and Jan Paegle, 1983: Observed and Modelled Long Wave Patterns of the Southern Hemisphere. Preprint Vol. of Extended Abstracts: First Inter. Conf. on S. Hemi. Meteor., July 31 - Aug. 6, 1983. Sao Jose Dos Campos, Brazil. American Meteorological Society, Boston, Mass., 37-40.

Petterssen, Sverre, 1969: Introduction to Meteorology. McGraw-Hill, Inc., 55-56, 267.

Sampson, G. W., 1982: Selected Analyses of the First Global Atmospheric Research Project Global Experiment Special Observation Period One Data. Master's Thesis, Depart. of Meteor., Univ. of Utah, 1-55.

Sikka, D. R., and S. Gadgil, 1980: On the Maximum Cloud Zone and the ITCZ over Indian Longitudes during the Southwest Monsoon. Mon. Wea. Rev., 108, 1840-1853.

Stern, William F., and Jeffrey J. Ploshay, 1983: An Assessment of GFDL's Continuous Data Assimilation System Used for Processing FGGE Data. Preprint Vol. of Extended Abstracts: Sixth Conf. on Numerical Wea. Prediction. June 6-9, 1983. Omaha, Nebr. American Meteorological Society, Boston, Mass., 90-95.

Susskind, J., J. Rosenfield, D. Reuter, and M. T. Chahine, 1984: Remote Sensing of Weather and Climate Parameters from HIRS2/MSU on TIROS-N. J. Geophys. Res., 89D (in press).

Trenberth, K. E., 1984: Interannual Variability of the Southern Hemisophere Circulation: Representativeness of the Year of the Global Weather Experiment. Mon. Wea. Rev., 112, 108-123.

Trenberth, K. E., and H. van Loon, 1981: Comment on "Impact of FGGE buoy data on Southern Hemisphere Analyses". Bull. Amer. Meteor. Soc., 62, 1486-1489.

Trewartha, Glenn T., 1968: An Introduction to Climate. McGraw-Hill, Inc., 394-395.

Wei, M. -Y., D. Johhnson, and R. D. Townsend, 1983: Seasonal Distributions of Diabatic Heating during the First GARP Global Experiment. Tellus, 35A, 241-255.

Yasunari, Tetsuzo, 1980: A Quasi-stationary Appearance of the 30 to 40 Day Period in the Cloudiness Fluctuations during the Summer Monsoon over India. J. Meteor. Soc. Japan, 58, 225-229.

Yasunari, Tetsuzo, 1981: Structure of an Indian Summer Monsoon System with Around 40-day Period. J. Meteor. Soc. Japan, 59, 336-354.

VITA

Name	Glenn David Ahrens
Birthdate	December 1, 1951
Birthplace	New Prague, Minnesota
High School	Belle Plaine, High School Belle Plaine, Minnesota
Colleges and Universities	St. Olaf College Northfield, Minnesota 1969-1973 University of Utah Salt Lake City, Utah 1973-1974, 1983-1984 South Plains College Levelland, Texas 1978-1979
Degrees	B.A., 1973 Chemistry and Religion St. Olaf College Northfield, Minnesota B.S., 1980 Meteorology University of Utah Salt Lake City, Utah
Professional Society	American Meteorological Society

END

FILMED

4-85

DTIC